Global Biogeochemical Cycles

RESEARCH ARTICLE
10.1029/2025GB008527

Impact of Atlantic Meridional Overturning Circulation Collapse on Carbon-13 Components in the Ocean

A. Schmittner[1]

[1]College of Earth, Ocean, and Atmospheric Sciences, Oregon State University, Corvallis, OR, USA

Key Points:

- Simulated collapse of the Atlantic Meridional Overturning Circulation affects atmospheric CO_2 and $\delta^{13}C_{CO2}$
- Largest effect on ocean $\delta^{13}C_{DIC}$ is in the deep North Atlantic, where remineralized and preformed components dominate
- Novel decomposition of $\delta^{13}C_{DIC}$ is accurate in transient simulations, whereas approximations based on Apparent Oxygen Utilization have large errors

Supporting Information:

Supporting Information may be found in the online version of this article.

Correspondence to:

A. Schmittner,
andreas.schmittner@oregonstate.edu

Citation:

Schmittner, A. (2025). Impact of Atlantic Meridional Overturning Circulation collapse on carbon-13 components in the ocean. *Global Biogeochemical Cycles*, *39*, e2025GB008527. https://doi.org/10.1029/2025GB008527

Received 30 JAN 2025
Accepted 3 NOV 2025

Author Contributions:

Conceptualization: A. Schmittner
Data curation: A. Schmittner
Formal analysis: A. Schmittner
Funding acquisition: A. Schmittner
Investigation: A. Schmittner
Methodology: A. Schmittner
Project administration: A. Schmittner
Resources: A. Schmittner
Software: A. Schmittner
Validation: A. Schmittner
Visualization: A. Schmittner
Writing – original draft: A. Schmittner
Writing – review & editing: A. Schmittner

Abstract Changes in the Atlantic Meridional Overturning Circulation (AMOC) are believed to have affected the cycling of carbon isotopes $(\delta^{13}C)$ in both the ocean and the atmosphere. However, understanding how AMOC changes $\delta^{13}C_{DIC}$ of Dissolved Inorganic Carbon (DIC) distributions in the ocean is limited, since models do not typically decompose the various processes that affect $\delta^{13}C_{DIC}$. Here, a new decomposition is applied to idealized simulations of an AMOC collapse, both for glacial and preindustrial conditions. The decomposition explicitly calculates the preformed and regenerated components of $\delta^{13}C_{DIC}$ and separates between physical and biological effects. An AMOC collapse leads to a large and rapid decrease in $\delta^{13}C_{DIC}$ in the North Atlantic, which is due to, in about equal parts, accumulation of remineralized organic matter and changes in preformed $\delta^{13}C_{DIC}$, both in glacial and preindustrial simulations. In the Pacific, Indian, and Southern Oceans $\delta^{13}C_{DIC}$ increases by a smaller magnitude. This increase is dominated by changes in preformed $\delta^{13}C_{DIC}$ in the glacial simulation and remineralized $\delta^{13}C_{DIC}$ in the preindustrial simulation. An extensive evaluation of the decomposition shows that its errors are small in most cases, especially for large basin-wide changes, whereas for small, local or global changes errors can be substantial. In contrast, approximations of the remineralized component based on Apparent Oxygen Utilization have large errors in most cases and are generally unreliable because they include contributions from oxygen disequilibrium.

1. Introduction

Large variations of the Atlantic Meridional Overturning Circulation (AMOC) are believed to have occurred in the past (Lynch-Stieglitz, 2017) and may be possible in the future due to global warming (Bakker et al., 2016; Rahmstorf, 2024; van Westen et al., 2024; Weijer et al., 2020). Millennial-scale AMOC variability during the last glacial cycle has been associated with aberrations in temperature (Buizert et al., 2024), atmospheric CO_2 (Ahn & Brook, 2008; Ahn et al., 2012), and carbon isotopes, both in the atmosphere (Bauska et al., 2016, 2018; Menking et al., 2022) and the ocean (Lynch-Stieglitz et al., 2019; Oppo et al., 2015; Repschläger et al., 2021). Here I consider the stable ^{13}C isotope, typically expressed in delta notation $\delta^{13}C = R/R_{std} - 1$, where $R = {}^{13}C/{}^{12}C$ is the ratio of heavy to light isotopes, relative to that of a standard R_{std}, and reported in parts per thousand, or permil.

However, the mechanistic links between AMOC, carbon (C) and $\delta^{13}C$ variations remain controversial. For example, the large decrease in $\delta^{13}C$ of Dissolved Inorganic Carbon (DIC), $\delta^{13}C_{DIC}$, in the deep North Atlantic during Heinrich Stadial 1, a cold event early during the last deglaciation associated with an AMOC reduction (McManus et al., 2004), has been attributed, on the one hand, to the accumulation of isotopically light respired organic carbon (Lacerra et al., 2017) and, on the other hand, to warming of sea surface temperatures, which affects preformed $\delta^{13}C$ through fractionation during air-sea gas exchange (Lynch-Stieglitz et al., 2019). Moreover, AMOC-related millennial-scale variability of CO_2 and $\delta^{13}C_{CO2}$ measured at high precision in Antarctic ice has been attributed to a variety of processes such as land carbon, Southern Ocean and North Atlantic gas exchange driven by sea ice or wind stress, and the ocean's biological carbon pump (Bauska et al., 2016, 2018; Menking et al., 2022). Although the $\delta^{13}C_{CO2}$ measurements provide constraints on mechanisms, they do not allow unequivocal attribution of CO_2 changes. For example, both land carbon loss and ocean respired carbon emissions would increase atmospheric CO_2 and decrease $\delta^{13}C_{CO2}$. Thus, additional data, such as $\delta^{13}C_{DIC}$ estimates from deep sea sediment cores and model simulations fitted to these data, are needed for improved understanding. Moreover, previous attribution studies used box models (Bauska et al., 2016, 2018; Menking et al., 2022), which can lead to different results compared to more complex spatially resolved models (Toggweiler, Gnanadesikan, et al., 2003; Toggweiler, Murnane, et al., 2003).

Although simulations with more complex interactive carbon cycle and $\delta^{13}C$ models have been conducted to explore the effects of AMOC variations (Menviel et al., 2015; Schmittner & Lund, 2015), the attribution of their $\delta^{13}C_{DIC}$ changes is complicated by different physical and biological mechanisms (Schmittner et al., 2013). Here, I apply a new method to decompose $\delta^{13}C_{DIC} = \Delta^{13}C_{pre} + \Delta^{13}C_{reg}$ into preformed and regenerated components, while separating biological and physical contributions to better understand the simulated changes. The method has previously been applied to equilibrium simulations of the Last Glacial Maximum (LGM, 20,000 years ago), demonstrating that the decomposition is precise and complete, and highlighting the importance of changes in biological disequilibrium components (Khatiwala et al., 2019; Schmittner & Fillman, 2024). Here, I apply the method for the first time to transient simulations, exploring the impacts of an AMOC shutdown. Since the method estimates preformed and regenerated components separately, it can be evaluated by comparing their sum with $\delta^{13}C_{DIC}$. The main goal of this paper is to provide a comprehensive evaluation of the method and illustrate changes in the spatial patterns of the different components. The same method has been applied to changes in DIC in a companion paper (Schmittner & Boling, 2025). Here, I focus on $\delta^{13}C_{DIC}$.

Approximations of regenerated components based on Apparent Oxygen Utilization (AOU) or phosphate have been frequently used (Lynch-Stieglitz et al., 1995; Menviel et al., 2015; Schmittner & Lund, 2015; Schmittner et al., 2013; Vollmer et al., 2022), but can have large errors in LGM equilibrium simulations (Khatiwala et al., 2019; Schmittner & Fillman, 2024). Here, I provide an additional assessment of those approximations by comparing them with the precise components calculated in transient simulations.

Recent studies indicate that the AMOC did not collapse completely during Heinrich Stadial 1 (HS1) (Oppo et al., 2015; Pöppelmeier et al., 2023; Repschläger et al., 2021), but quantifying AMOC changes in the paleo ocean remains a challenge and it is unknown whether a complete AMOC collapse occurred during previous events. Thus, my simulations, which use LGM initial conditions and simulate an AMOC collapse, are idealized experiments and not realistic simulations of HS1. For this reason, I also do not attempt a detailed comparison with paleo data here. Nevertheless, I hope the results may be useful in interpreting past observed changes. More realistic simulations, including detailed comparisons to paleo data, will be left for future studies.

2. Methods

2.1. Model Description

The Oregon State University version of the University of Victoria climate model (OSU-UVic) version 2.9.10 is used as in Schmittner and Fillman (2024). Its three-dimensional ocean component is coupled with a computationally efficient atmospheric energy moisture balance model, a land surface and vegetation module, a dynamic-thermodynamic sea ice component, and the process-based Model of Ocean Biogeochemistry and Isotopes (MOBI), all run at a coarse resolution of 1.8 × 3.6° with 19 vertical levels. MOBI includes four plankton functional types (diatoms, diazotrophs, other phytoplankton and zooplankton), nutrients (nitrate, phosphate, silicate and iron), semi-refractory dissolved organic carbon (Somes & Oschlies, 2015), and variable stoichiometry (Fillman et al., 2023). C and ^{13}C are tracked in ocean, land, and atmospheric components. Details of the ^{13}C implementation are provided by Schmittner et al. (2013). Note that the model version used here does not include interactive sediments and permafrost. Thus, a closed-system approach is taken with regard to C and ^{13}C, which are conserved in the land-atmosphere-ocean system after model spinup (see below). This approximation should be valid for millennial timescales, which will be the focus of this paper, since sediment interactions are believed to play a role only on timescales longer than about 5,000 years (Archer et al., 1998).

The atmospheric component uses prescribed seasonally varying winds and atmospheric co-albedo (Weaver et al., 2001), rather than interactive winds and clouds. This is a caveat, as changes in AMOC are expected to affect winds and clouds, which could modulate C and ^{13}C on land and in the surface ocean (Buizert et al., 2018; Chiang & Bitz, 2005; Frierson et al., 2013). The advantage of using such a simple atmospheric component is that the model is computationally efficient, which allows multiple millennial scale simulations and sensitivity tests. Changes in winds are considered in the LGM simulations, by applying anomalies from models with dynamic atmospheres (Muglia & Schmittner, 2015). Model results have been extensively validated against present day observations and reconstructions from the LGM as described in more detail in the Supporting Information S1. Here I mainly use as initial conditions an equilibrated data-constrained LGM version (Khatiwala et al., 2019;

Table 1
Components of $\delta^{13}C_{DIC}$

Abbreviation	Calculation	Description
$DI^{13}C$	DC (*Full*)	Total Dissolved Inorganic Carbon-13
$^{13}C_{pre}$	DC (*Full*)	Preformed Carbon-13
$^{13}C_{sat}$	DC (*Full*)	Saturation Carbon-13
$^{13}C_{dis}$	$^{13}C_{pre} - {}^{13}C_{sat}$	Disequilibrium Carbon-13
$^{13}C_{pre,phy}$	DC (*NoBio*)	Physical Preformed Carbon-13
$^{13}C_{sat,phy}$	DC (*NoBio*)	Physical Saturation Carbon-13
$^{13}C_{dis,phy}$	$^{13}C_{pre,phy} - {}^{13}C_{sat,phy}$	Physical Disequilibrium Carbon-13
$^{13}C_{pre,bio}$	$^{13}C_{pre} - {}^{13}C_{pre,phy}$	Biological Preformed Carbon-13
$^{13}C_{sat,bio}$	$^{13}C_{sat} - {}^{13}C_{sat,phy}$	Biological Saturation Carbon-13
$^{13}C_{dis,bio}$	$^{13}C_{dis} - {}^{13}C_{dis,phy}$	Biological Disequilibrium Carbon-13
$^{13}C_{soft}$	DC (*Full*)	Soft-Tissue Carbon-13
$^{13}C_{caco3}$	DC (*Full*)	Calcium Carbonate Carbon-13
$^{13}C_{reg}$	$^{13}C_{soft} + {}^{13}C_{caco3}$	Regenerated Carbon-13
$^{13}C_{bio}$	$^{13}C_{reg} + {}^{13}C_{pre,bio}$	Biological Carbon-13
R_x	$^{13}C_x / {}^{12}C_x$	Isotope Ratio of Component x
$\delta^{13}C_x$	$R_x / R_{std} - 1$	Small Delta Value of Component x
$\Delta^{13}C_x$	$C_x \delta^{13}C_x / DIC$	Contribution of Component x to $\delta^{13}C_{DIC}$
$\Delta^{13}C_{soft,AOU}$	$AOU(-1.1)/170$*	AOU Approximation of $\Delta^{13}C_{soft}$
$^{13}\Sigma$	$\Delta^{13}C_{pre} + \Delta^{13}C_{reg}$	Sum of Components
$^{13}\epsilon$	$^{13}\Sigma - \delta^{13}C_{DIC}$	Error of Decomposition

Note. Directly calculated (DC) components are indicated in the second column with the model in brackets. Total components are calculated using the *Full* model, which includes both physics and biology. Physical components are calculated using model *NoBio*, which excludes biology. Formulas are provided for derived components. Since model *NoBio* has no regenerated components physical carbon-13 $^{13}C_{phy} = {}^{13}C_{phy,pre}$ is only preformed. (*) From Vollmer et al. (2022), $AOU = O_{2,sat} - O_2$ is the deviation of the dissolved oxygen concentration O_2 from its temperature-dependent saturation value $O_{2,sat}$ in mmol/m^3.

Muglia et al., 2017; Schmittner & Fillman, 2024). Thus, most of the simulations described here represent glacial climates of the Pleistocene, although some results from preindustrial runs are also included.

2.2. Ocean Carbon-13 Decomposition

For the decomposition of $\delta^{13}C_{DIC}$ I explicitly track $^{13}C_{pre}$, $^{13}C_{sat}$, $^{13}C_{soft}$ and $^{13}C_{caco3}$ (Table 1) and their respective ^{12}C counterparts. The regenerated components ($^{13}C_{reg} := {}^{13}C_{soft} + {}^{13}C_{caco3}$) from the remineralization of soft-tissue organic matter ($^{13}C_{soft}$) and dissolution of calcium carbonate ($^{13}C_{caco3}$) are calculated directly by accumulating the model's DI^{13}C sources in the interior, while setting surface concentrations to zero. Preformed ($^{13}C_{pre}$) and saturation ($^{13}C_{sat}$) components are equal to the surface concentrations of DI^{13}C and DI$^{13}C_{sat}$, respectively, and then propagated into the interior with zero subsurface sources and sinks (Schmittner & Fillman, 2024). Disequilibrium components, $^{13}C_{dis} := {}^{13}C_{pre} - {}^{13}C_{sat}$, are calculated from the differences between preformed and saturation components. As in Schmittner and Fillman (2024), I use the capital delta notation, for example, $\Delta^{13}C_{pre} := C_{pre}\delta^{13}C_{pre}/DIC$, to indicate components of $\delta^{13}C_{DIC}$ weighted by their relative DIC content, which are additive, for example, $\delta^{13}C_{DIC} = \Delta^{13}C_{pre} + \Delta^{13}C_{reg}$, in contrast to the small delta values, for example, $\delta^{13}C_{DIC} \neq \delta^{13}C_{pre} + \delta^{13}C_{reg}$. Since preformed and regenerated components are computed independently, their sum $^{13}\Sigma := \Delta^{13}C_{pre} + \Delta^{13}C_{reg}$ should approximate $\delta^{13}C_{DIC}$ and the difference $^{13}\epsilon = {}^{13}\Sigma - \delta^{13}C_{DIC}$ is a measure of the error of the decomposition, which I will use here to evaluate the method.

Due to biological fractionation during photosynthesis, organic matter has a large negative delta value $\delta^{13}C_{org} \simeq -22‰$ and $\Delta^{13}C_{soft}$ is negative. It's global mean value is $-0.73‰$ in our model's preindustrial ocean and $-0.56‰$ in the LGM (Schmittner & Fillman, 2024). In contrast, calcium carbonate production does not fractionate, and thus the $\delta^{13}C_{CaCO3} \simeq 2‰$ is close to the surface value of $\delta^{13}C_{DIC}$ and $\Delta^{13}C_{CaCO3} \simeq 0.03$–$0.04‰$ (global mean LGM and PI, respectively) is small.

In addition to the main experiments, which are referred to as *LGM Full* in the following, two other model versions have been constructed. Ocean biology has been removed in model *LGM NoBio* and the influence of changes in land carbon on the atmosphere has been deactivated in model *LGM NoLand* by setting to zero C and ^{13}C fluxes between the atmosphere and the land in the calculation of atmospheric CO_2 and $\delta^{13}C_{CO2}$. Thus, model *LGM NoLand* represents an ocean-atmosphere-only carbon cycle, which is useful, compared to model *LGM Full*, in quantifying contributions to atmospheric CO_2 changes from land carbon variations. Model *LGM NoBio* represents a physics-only ocean carbon cycle and yields the physical components of the decomposition, for example, $C_{dis,phy}$. Biological components are diagnosed as the difference from the *LGM Full* model, for example, $C_{dis,bio} = C_{dis} - C_{dis,phy}$.

The biological disequilibrium component arises, for example, from upwelling of respired carbon, which is isotopically light. Air-sea gas exchange will lead to increasing isotope ratios. If the air-sea equilibration is incomplete, as is the case in the Southern Ocean, then the water returning to the subsurface will have an excess of light isotopes. Thus, $\Delta^{13}C_{dis,bio}$ is negative almost everywhere in the ocean. Its global mean values in the PI and LGM model are -0.70 and $-1.37‰$, respectively. The physical disequilibrium arises, for example, from upwelling of relatively warm waters in the Antarctic divergence and cooling of that water as it moves south. This leads to increases in the isotope ratio due to the temperature-dependent fractionation during air-sea gas exchange (Zhang et al., 1995). Since equilibration is incomplete, the waters that subduct back into the interior as Antarctic Bottom Water (AABW) have a lower isotope ratio than they would at equilibrium. Thus, $\Delta^{13}C_{dis,phy}$ is negative in AABW and other deep water masses. Its global mean values in the PI and LGM are -1.42 and $-1.48‰$, respectively (Schmittner & Fillman, 2024). The biological saturation component $\Delta^{13}C_{sat,bio}$ is small (-0.07 to $-0.08‰$ in PI and LGM, respectively). In contrast, $\Delta^{13}C_{sat,phy}$ is large and positive due to the temperature-dependent fractionation during air-sea gas exchange. Cooler temperatures, for example, increase the $\Delta^{13}C_{sat,phy}$ to $\sim 4‰$ in the polar oceans, while warm temperatures lead to values of $\sim 1‰$ in the tropics. More details on the different components and how they change in LGM simulations can be found in Schmittner and Fillman (2024). Spatial distributions of the components will be shown below. Results will also be shown from a models with preindustrial background climate, referred to as *PI Full* and *PI NoBio*.

Thus, the full decomposition for $\delta^{13}C_{DIC}$ is

$$\delta^{13}C_{DIC} = \Delta^{13}C_{soft} + \Delta^{13}C_{caco3} + \Delta^{13}C_{sat,phy} + \Delta^{13}C_{sat,bio} + \Delta^{13}C_{dis,phy} + \Delta^{13}C_{dis,bio} - {}^{13}\epsilon. \quad (1)$$

2.3. Model Spin-Up and Experimental Design

The models are spun up in stages as in Schmittner and Fillman (2024). Following a 7000-year phase with prescribed CO_2 and other forcings at preindustrial conditions, CO_2 is allowed to vary according to land-atmosphere and ocean-atmosphere carbon fluxes. Once equilibrated, LGM boundary conditions are imposed instantaneously, leading to a decrease in CO_2, cooling of global temperatures, and a shallower and weaker AMOC compared to the preindustrial simulation. Model *LGM NoBio* was equilibrated with an atmospheric CO_2 concentration of 190 ppm and $\delta^{13}C_{CO2} = -6.5‰$ for 6,000 years, followed by a 1,000-year phase with prognostic CO_2 and $\delta^{13}C_{CO2}$, leading to an almost identical climate as the model *LGM Full*. Note that this spinup procedure leads to different carbon and ^{13}C inventories in models *LGM Full* and *LGM NoBio*, since model *LGM NoBio* has no biological carbon. Cooling of global surface air temperatures in both models is 5.7°C, comparable with two recent observation-based estimates (-6.1 ± 0.2°C and -4.5 ± 0.9°C) (Annan et al., 2022; Tierney et al., 2020).

The freshwater hosing experiments conducted here to perturb the AMOC are similar to previous work. Results regarding physics, the carbon cycle, and $\delta^{13}C$ are comparable to Schmittner et al. (2007) and Schmittner and

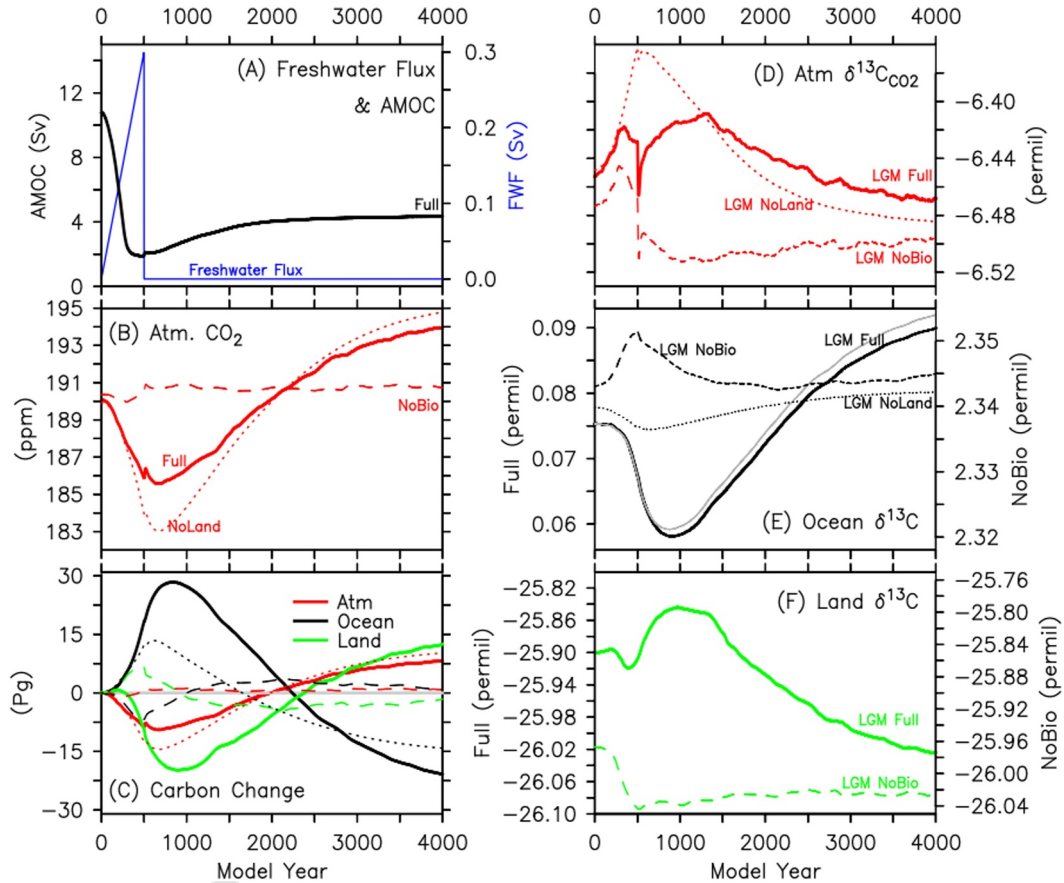

Figure 1. Freshwater flux and response of circulation (a), global carbon (b, c) and ^{13}C (d–f) cycles to AMOC collapse in LGM climate. In panel (a) the AMOC in *LGM NoBio* is indistinguishable from *LGM Full*. (d) $\delta^{13}C_{CO2}$ of atmospheric CO_2. (e) Ocean $\delta^{13}C_{ocn} = \left(\delta^{13}C_{DIC}DIC + \delta^{13}C_{DOC}DOC\right)/(DIC + DOC)$ is the weighted average of $\delta^{13}C$ of DIC and DOC. The gray line shows the changes of $\delta^{13}C_{DIC}$ with respect to $\delta^{13}C_{ocn}(t = 0)$. The range of the vertical axes is 0.037‰. (f) Land $\delta^{13}C_{lnd} = \left(\delta^{13}C_{veg}C_{veg} + \delta^{13}C_{soil}C_{soil}\right)/(C_{veg} + C_{soil})$ is the weighted average of $\delta^{13}C$ of soil (C_{soil}) and vegetation (C_{veg}) carbon. The range of the vertical axes is 0.3‰. Results from model *LGM Full* (thick solid lines, left axes), *LGM NoBio* (dashed, right axis) and *LGM NoLand* (dotted, left axis).

Lund (2015) and will not be discussed in detail here. I apply a freshwater flux into the North Atlantic that linearly increases from zero at (arbitrary) model year 0–0.3 Sv at model year 500 after which it is set to zero (Figure 1a).

3. Results

3.1. Response of Global $\delta^{13}C$ Inventories

In response to increasing freshwater fluxes and reducing AMOC (Figure 1a), atmospheric CO_2 first decreases and then increases (Figure 1b) due to changes in ocean carbon (Figure 1c) as discussed in more detail in the companion paper. $\delta^{13}C_{CO2}$ in model *LGM Full* increases from −6.453‰ in year 0 to −6.420‰ at year 300, at which time it starts to decrease, culminating in an abrupt drop of about −0.04‰ at year 500 Figure 1d). The subsequent resumption until year 1300 is followed by a gradual decline until year 4,000. Comparison with model *LGM NoLand* reveals that the initial increase up to year 300 is caused by the ocean, whereas the subsequent decrease and drop at year 500 in model *LGM Full* are caused by changes in land carbon. Ocean-only changes in model *LGM NoLand* lead to a smooth but rapid increase in $\delta^{13}C_{CO2}$ by about 0.09‰ until about year 500 and a slow and smooth decrease thereafter, reaching a value of −6.484‰ at year 4,000, just slightly lower than in model *LGM Full* (−6.468‰) and the initial condition. The standard deviation of $\delta^{13}C_{CO2}$ in *LGM NoLand* is with $\sigma = 0.038$‰ twice as large as that in *LGM Full* although its evolution is smoother due to the absence of the

abrupt event around year 500. Model *LGM NoBio* shows a similar abrupt drop around year 500 but without the subsequent recovery exhibited by model *LGM Full*.

The globally averaged $\delta^{13}C$ of the ocean $\left(\delta^{13}C_{ocn}\right)$ decreases after about year 300 from 0.075 to 0.058‰ around year 900, after which it slowly increases to 0.09‰ at year 4,000 (Figure 1e). The larger initial increase in $\delta^{13}C_{CO2}$ in model *LGM NoLand* drives the ocean $\delta^{13}C$ higher, and thus the response in $\delta^{13}C_{ocn}$ in model *LGM NoLand* is strongly muted, compared to model *LGM Full*. The response of $\delta^{13}C_{ocn}$ in model *LGM NoBio* is also muted but shows an initial increase followed by a decrease, opposite to the changes in the other two models. This indicates that physical changes in the ocean in these models drive $\delta^{13}C_{ocn}$ initially higher, but have little impact on long-term changes, which implies that changes in biological carbon storage dominate the response in model *LGM Full*.

The whole ocean $\delta^{13}C_{DIC}$ in model *LGM NoBio* is more than 2‰ higher than that of model *LGM Full* (Figure 1e) because surface values of $\delta^{13}C_{DIC}$ are around 2.6‰ and they decrease only slightly with depth due to the missing input of isotopically light organic carbon (e.g., Figure 4d in Schmittner & Fillman, 2024). At saturation, deep-ocean values would be even higher, around 3.6‰ due to temperature-dependent fractionation during air-sea gas exchange.

The similarity of the variations of land $\delta^{13}C$ $\left(\delta^{13}C_{lnd}\right)$ with those of $\delta^{13}C_{CO2}$ in models *LGM Full* and *LGM NoBio* indicates the strong influence of the atmosphere on $\delta^{13}C_{lnd}$ (Figure 1f). However, the long-term decline in $\delta^{13}C_{lnd}$ is greater than in the atmosphere, indicating that climate-driven changes in the composition of C3 and C4 plants also play a role, similar to previous simulations (Schmittner & Lund, 2015, their Figure 3).

3.2. Ocean Carbon-13 Decomposition

3.2.1. Temporal Global and Basin-Wide Changes

Because changes in the simulated global mean $\delta^{13}C_{ocn}$ are dominated by $\delta^{13}C_{DIC}$ (compare gray and black solid lines in Figure 1e) I will focus the analysis on $\delta^{13}C_{DIC}$. In year zero, the global mean of the sum of the components ${}^{13}\Sigma := \Delta^{13}C_{pre} + \Delta^{13}C_{reg}$ is 0.169‰, which is close to the global mean of $\delta^{13}C_{DIC}$ (0.158‰) considering that the spatial variations in $\delta^{13}C_{DIC}$ are about 2‰ and temporal variations of global mean $\delta^{13}C_{DIC}$ on glacial-interglacial time scales are approximately 0.3‰ (Gebbie et al., 2015). The sum of the components also tracks well the evolution of the $\delta^{13}C_{DIC}$ changes in model *LGM Full* (solid red and black curves in Figure 2a), which first decreases by about 0.015‰ until year 1,000 after which it increases by about 0.025‰ until the year 4,000. However, during the second half of the simulation the sum of the components overestimates the changes by about 0.005‰, indicating that the decomposition is imperfect, especially on the global scale, and if the changes in $\delta^{13}C_{DIC}$ are relatively small.

The decomposition shows that the global mean change in $\delta^{13}C_{DIC}$ is the relatively small residual of large opposing changes in preformed and regenerated components. Whereas $\Delta^{13}C_{reg}$ decreases, $\Delta^{13}C_{pre}$ increases. The initial decrease in $\delta^{13}C_{DIC}$ until year 1,000 is dominated by a large and rapid decrease in $\delta^{13}C_{soft}$ by about 0.05‰, which peaks around year 1,300. $\delta^{13}C_{caco3}$ changes are negligible throughout this paper and will not be discussed further. The initial decrease in $\delta^{13}C_{soft}$ is largely, but not fully, compensated for by an increase in the preformed component by about 0.04‰ until year 1,500. This increase is dominated by physical disequilibrium changes, while saturation changes are smaller due to compensation of physical and biological saturation. These changes in the preformed components are qualitatively different from the DIC components, which show more important contributions from the saturation component during the first half of the simulation and increasing contributions from the biological disequilibrium during the second half of the simulation (companion paper, Figure 3).

The AOU approximation underestimates $\Delta^{13}C_{soft}$ in year 0 by almost 1‰, consistent with Schmittner and Fillman (2024), but it accurately reproduces the simulated changes of $\Delta^{13}C_{soft}$ until about year 1,000 (Figure 2c). After that, $\Delta^{13}C_{soft,AOU}$ results in a much larger increase than C_{soft}, such that at the end of the simulation $\Delta^{13}C_{soft,AOU}$ is 0.025‰ larger than in year 0, while $\Delta^{13}C_{soft}$ is −0.028‰ smaller. Thus, the AOU approximation results in a wrong sign of the changes with respect to year 0.

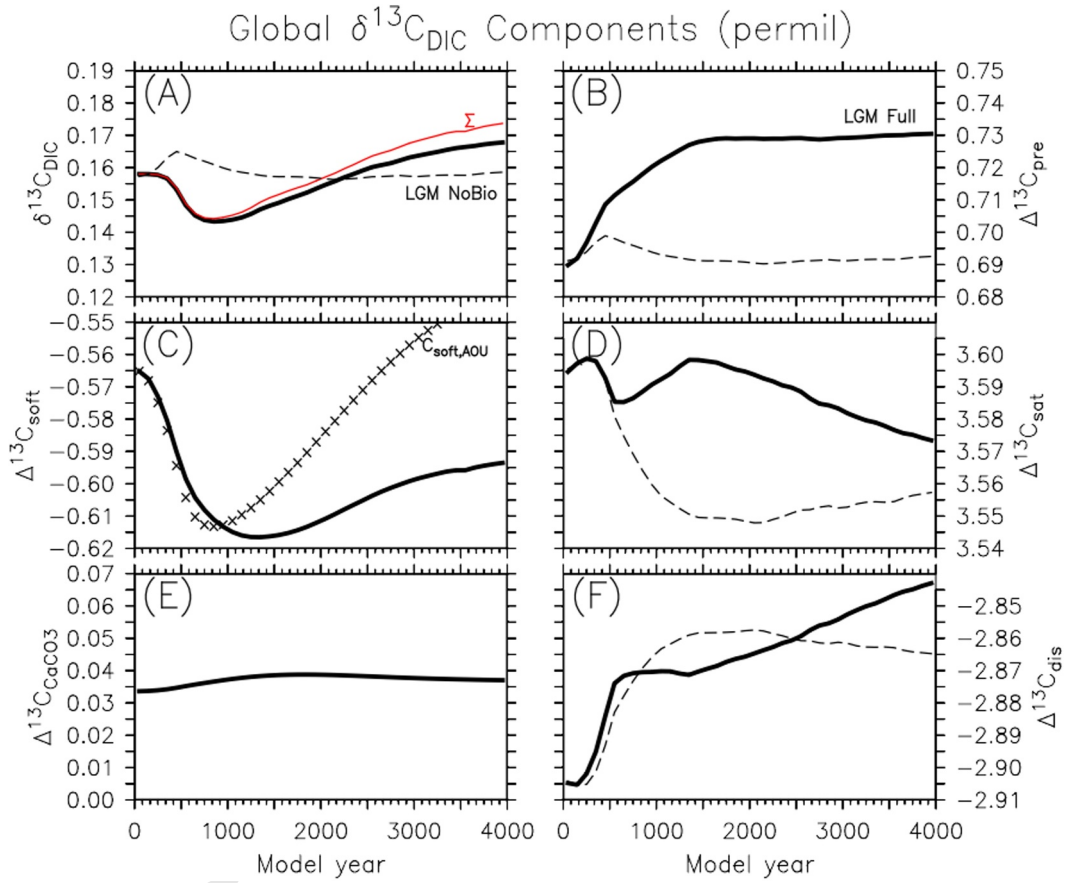

Figure 2. Global $\delta^{13}C_{DIC}$ components in models *LGM Full* (thick solid) and *LGM NoBio* (dashed). The range of the vertical axes is 0.07‰ in all panels. (a) $\delta^{13}C_{DIC}$ (black) and the change ${}^{13}\Sigma(t)-{}^{13}\Sigma(t=0)+\delta^{13}C_{DIC}(t=0)$ in the sum of the components ${}^{13}\Sigma := \Delta^{13}C_{pre}+\Delta^{13}C_{reg}$ adjusted for the difference between ${}^{13}\Sigma$ and $\delta^{13}C_{DIC}$ at $t=0$ (red). (b) $\Delta^{13}C_{pre}$. (c) $\Delta^{13}C_{soft}$ (line) and $\Delta^{13}C_{soft,AOU}$ adjusted by the difference $\delta^{13}C_{soft,AOU}(t=0)-\delta^{13}C_{soft}(t=0)=-0.945‰$ at year 0 (symbols). Results from model *LGM NoBio* have been adjusted for the differences with *LGM Full* at year 0. For reference, $\delta^{13}C_{DIC,NoBio}(t=0)=\Delta^{13}C_{phy}(t=0)=\Delta^{13}C_{pre,phy}(t=0)=2.31‰$, $\Delta^{13}C_{soft,AOU}(t=0)=-1.51‰$, $\Delta^{13}C_{sat,NoBio}(t=0)=\Delta^{13}C_{sat,phy}(t=0)=3.90‰$, $\Delta^{13}C_{dis,NoBio}(t=0)=\Delta^{13}C_{dis,phy}(t=0)=-1.59‰$.

Similarly to carbon, as illustrated in Figures 4 and 5 of the companion paper, the relatively small changes in the mean $\Delta^{13}C_{DIC}$ of the global ocean are the net result of large redistributions between the different ocean basins (Figures 3 and 4). $\Delta^{13}C_{DIC}$ in the Atlantic rapidly decreases by 0.5‰ until year 1,000, peaks around year 1,400 at 0.186‰, and subsequently recovers slightly by 0.05‰ until year 4,000. In contrast, the mean $\Delta^{13}C_{DIC}$ in the Pacific, Indian and Southern Oceans initially increases rapidly by about 0.1‰ until year 1,000, after which it slowly increases by an additional 0.02‰ until year 4,000.

The decomposition is much more accurate for the basin-wide changes compared with the global ocean changes. The sum of the components follows very closely $\Delta^{13}C_{DIC}$ in all ocean basins. In the Atlantic, ${}^{13}\Sigma$ overestimates the decrease in $\Delta^{13}C_{DIC}$ by 0.014‰ at year 1,000, which corresponds to 3% of the $\Delta^{13}C_{DIC}$ changes since year 0. Similarly for the Pacific, Indian and Southern Oceans, ${}^{13}\Sigma$ underestimates changes by up to 0.005‰ at year 4,000, or 4% of the $\Delta^{13}C_{DIC}$ changes since year 0.

In contrast, the AOU approximation overestimates the decrease of $\Delta^{13}C_{soft}$ in the Atlantic by up to −0.19‰ in year 800, which corresponds to 83% of the changes from year 0, although the shapes of the curves are similar. In the Pacific, Indian and Southern Oceans $\Delta^{13}C_{soft}$ does not change much, increasing by only 0.02‰ until year 4,000, while $\Delta^{13}C_{soft,AOU}$ increases substantially by 0.12‰.

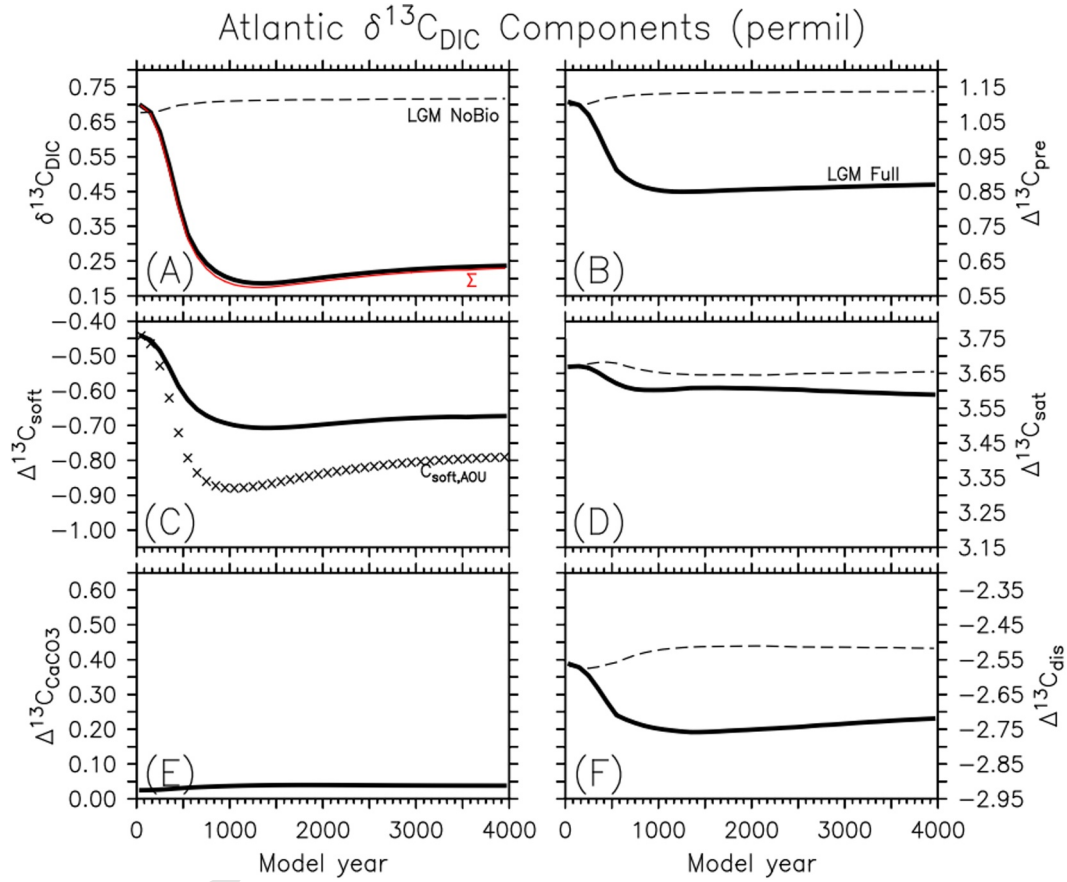

Figure 3. As Figure 2 but for Atlantic north of 40°S. The range of the vertical axis is 0.65‰ in all panels. $^{13}\Sigma(t=0) = 0.61‰$, $\Delta^{13}C_{phy}(t=0) = \Delta^{13}C_{pre,phy}(t=0) = 2.28‰$, $\Delta^{13}C_{soft,AOU}(t=0) = -1.08‰$, $\Delta^{13}C_{sat,phy}(t=0) = 3.84‰$, $\Delta^{13}C_{dis,phy}(t=0) = -1.57‰$.

Whereas $\Delta^{13}C_{soft}$ does not change much in the Pacific, Indian and Southern Oceans, in the Atlantic it decreases by −0.25‰ until year 1,000, and stays constant afterward. In the Atlantic, changes in $\Delta^{13}C_{pre}$ are quite similar. Thus, in the Atlantic, $\Delta^{13}C_{pre}$ and $\Delta^{13}C_{soft}$ conspire to decrease $\Delta^{13}C_{DIC}$. The initial decrease in $\Delta^{13}C_{pre}$ in the Atlantic is dominated by $\Delta^{13}C_{dis,bio}$.

These basin-average changes are opposite to those in the carbon components as illustrated in Figures 4 and 5 of the companion paper. One difference is the saturation component, which changes more in the Pacific for carbon. Another difference is that for carbon, the physical preformed components change much less than for $\delta^{13}C$, for which they show opposite signs, such that $\Delta^{13}C_{sat,phy}$ decreases while $\Delta^{13}C_{dis,phy}$ increases.

3.2.2. Spatial Distributions

Due to the strong temperature-dependent fractionation during air-sea gas exchange, saturation values in the deep ocean are higher than on the surface (Figure 5). However, they do not change much as the AMOC is reduced, in contrast to the preformed component, which decreases in the Atlantic and increases in the Pacific, thus being the dominant component for the changes in $\delta^{13}C_{DIC}$. The large differences between $\Delta^{13}C_{sat}$ and $\Delta^{13}C_{pre}$ imply an important role for disequilibrium changes.

Horizontally averaged $\delta^{13}C_{DIC}$ decreases by up to 1.1‰ at 2 km depth in the Atlantic, with similar contributions from $\Delta^{13}C_{pre}$ and $\Delta^{13}C_{soft}$, although the latter contributions are slightly smaller. In the Pacific, Indian and Southern Oceans horizontally averaged $\delta^{13}C_{DIC}$ increases by up to 0.2‰ around 1.4 km depth, and below 3 km by

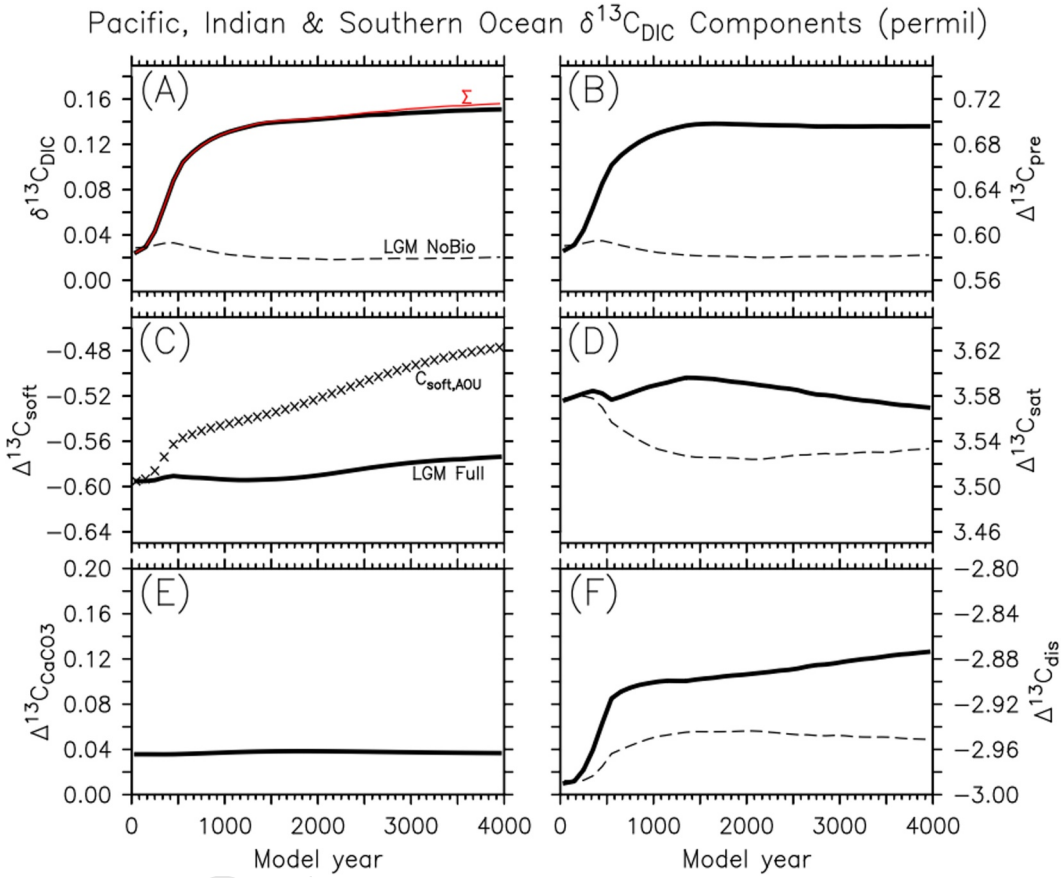

Figure 4. As Figure 3 but for the Pacific, Indian and Southern Oceans including the Atlantic south of 40°S. $^{13}\Sigma(t=0) = 0.038‰$, $\Delta^{13}C_{phy}(t=0) = \Delta^{13}C_{pre,phy}(t=0) = 2.32‰$, $\Delta^{13}C_{soft,AOU}(t=0) = -1.62‰$, $\Delta^{13}C_{sat,phy}(t=0) = 3.92‰$, $\Delta^{13}C_{dis,phy}(t=0) = -1.60‰$.

around 0.1‰. Changes there are dominated by $\Delta^{13}C_{pre}$, whereas $\Delta^{13}C_{soft}$ contributions are only important in the upper 1.5 km.

The sum of the components provides an excellent approximation of the horizontally averaged $\delta^{13}C_{DIC}$ changes. In contrast, the AOU approximation overestimates changes in the Atlantic and in the other ocean basins by large amounts.

The decrease in $\delta^{13}C_{DIC}$ in the Atlantic around 2 km is focused between 30 and 60°N with amplitudes of up to −2‰ (Figure 6). Changes are much smaller and positive in the Indian and Pacific Oceans, exceeding 0.6‰ only in the far North Pacific around 1 km depth. The pattern of $\delta^{13}C_{DIC}$ change is opposite to that of DIC (Figure 7 in companion paper). The large difference in $\delta^{13}C_{DIC}$ values between the North Atlantic and the North Pacific above ~3 km depth in year 0 (panels D and G in Figure 6), which is due to differences in deep water formation, is erased by the AMOC shutdown (panels E and H in Figure 6). In the AMOC-on state, $\delta^{13}C_{DIC}$ values in the Atlantic are much lower than in the Pacific (Figures 6d and 6g) due to strong vertical mixing and downward transport of high $\delta^{13}C_{DIC}$ surface waters to depths in the Atlantic, whereas in the Pacific strong stratification inhibits vertical mixing and allows for the accumulation of low respired $\Delta^{13}C_{soft}$ (Figure 8g). Preformed values are also higher in the deep Atlantic, compared to the deep Pacific (Figures 9d and 9g). Thus, as a consequence of the AMOC shutdown and increasing stratification in the North Atlantic, the Atlantic becomes more like the Pacific (Figures 6e and 6h), and $\delta^{13}C_{DIC}$ (Figure 6f), $\Delta^{13}C_{soft}$ (Figure 8f) and $\Delta^{13}C_{pre}$ (Figure 9f) decrease at mid depths in the North Atlantic.

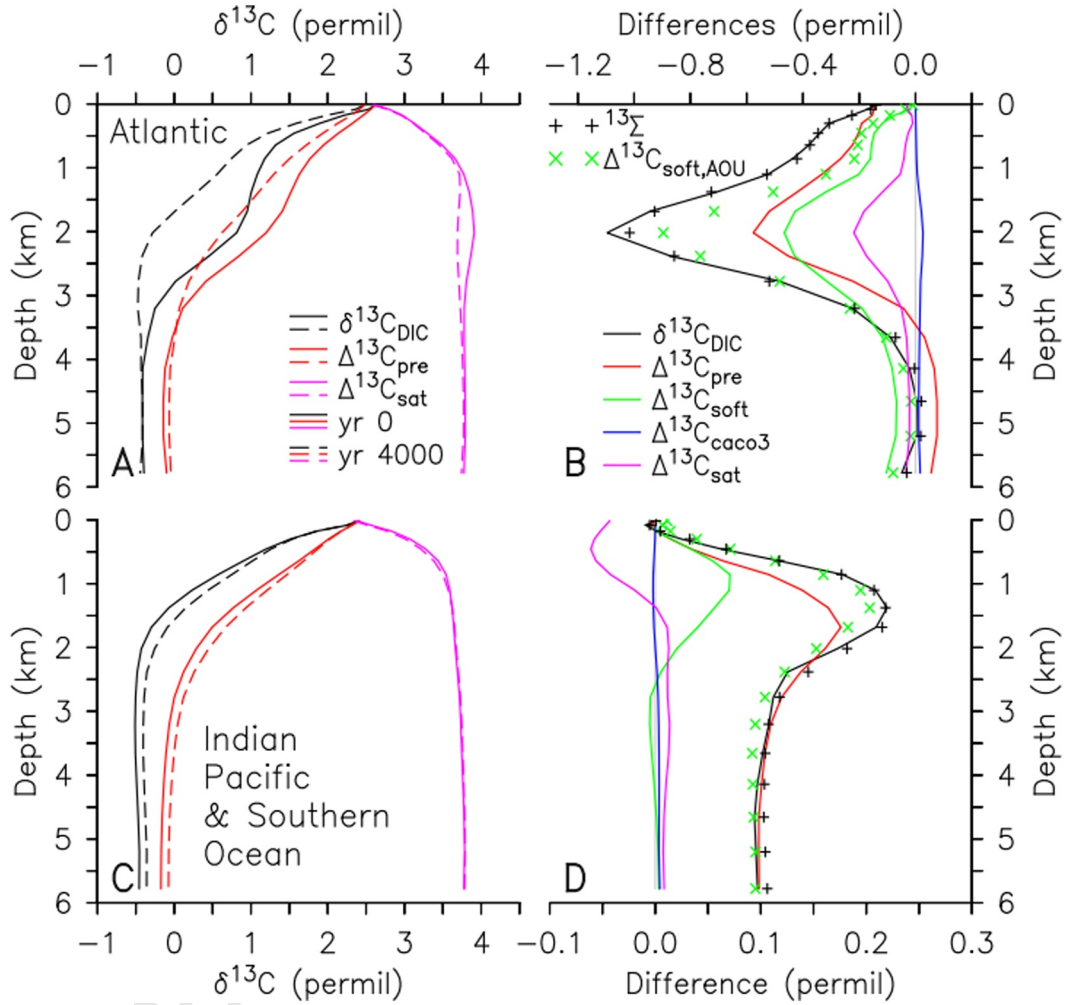

Figure 5. Horizontally averaged components of $\delta^{13}C_{DIC}$ in the Atlantic (a, b) and Indian, Pacific and Southern Oceans (c, d) in model *LGM Full*. (a, c) show absolute values of $\delta^{13}C_{DIC}$ (black), $\Delta^{13}C_{pre}$ (red) and $\Delta^{13}C_{sat}$ (purple) at years 0 (solid, AMOC on) and 4,000 (dashed, AMOC off). (b, d) Show differences (yr 4,000 minus yr 0) for $\delta^{13}C_{DIC}$ (black), $\Delta^{13}C_{pre}$ (red), $\Delta^{13}C_{soft}$ (green), $\Delta^{13}C_{caco3}$ (blue), C_{sat} (purple), $^{13}\Sigma$ (black + symbols) and $\Delta^{13}C_{soft,AOU}$ (green x symbols).

The errors of the decomposition $^{13}\epsilon := {}^{13}\Sigma - \delta^{13}C_{DIC}$ are largest in the thermocline of the northern Indian Ocean, where they exceed 0.2‰ (Figure 7). However, in most of the ocean outside the tropical thermocline, errors are smaller than 0.05‰, indicating that the decomposition is accurate. The errors do not change much over the course of the simulation. The greatest changes occur in the tropical North Atlantic around 2 km depth, where $^{13}\epsilon$ increases by up to 0.1‰. Compared with the amplitude of the $\delta^{13}C_{DIC}$ changes of around 1‰ there, the error is less than 10%. In most of the ocean, the changes in $^{13}\epsilon$ are less than 0.05‰.

3.2.3. Regenerated Components

Mirroring C_{soft} (Figure 9 in companion paper), the distribution of $\Delta^{13}C_{soft}$ at model year 0 is characterized by minima at the equator around 500 m depth and in the North Pacific around 1,500 m, where the accumulation of isotopically light, respired carbon in waters that have been isolated from the surface for a long time has decreased $\delta^{13}C_{DIC}$, while values in the North Atlantic at that depth are close to zero (Figure 8). The latter is, of course, due to the formation of deep water in the North Atlantic, where the advection of surface waters with near-zero $\Delta^{13}C_{soft}$ causes less negative values at depth compared to the North Pacific. Consequently, the collapse of the AMOC leads to a large decrease in $\Delta^{13}C_{soft}$ in the North Atlantic as isotopically light remineralized organic carbon accumulates

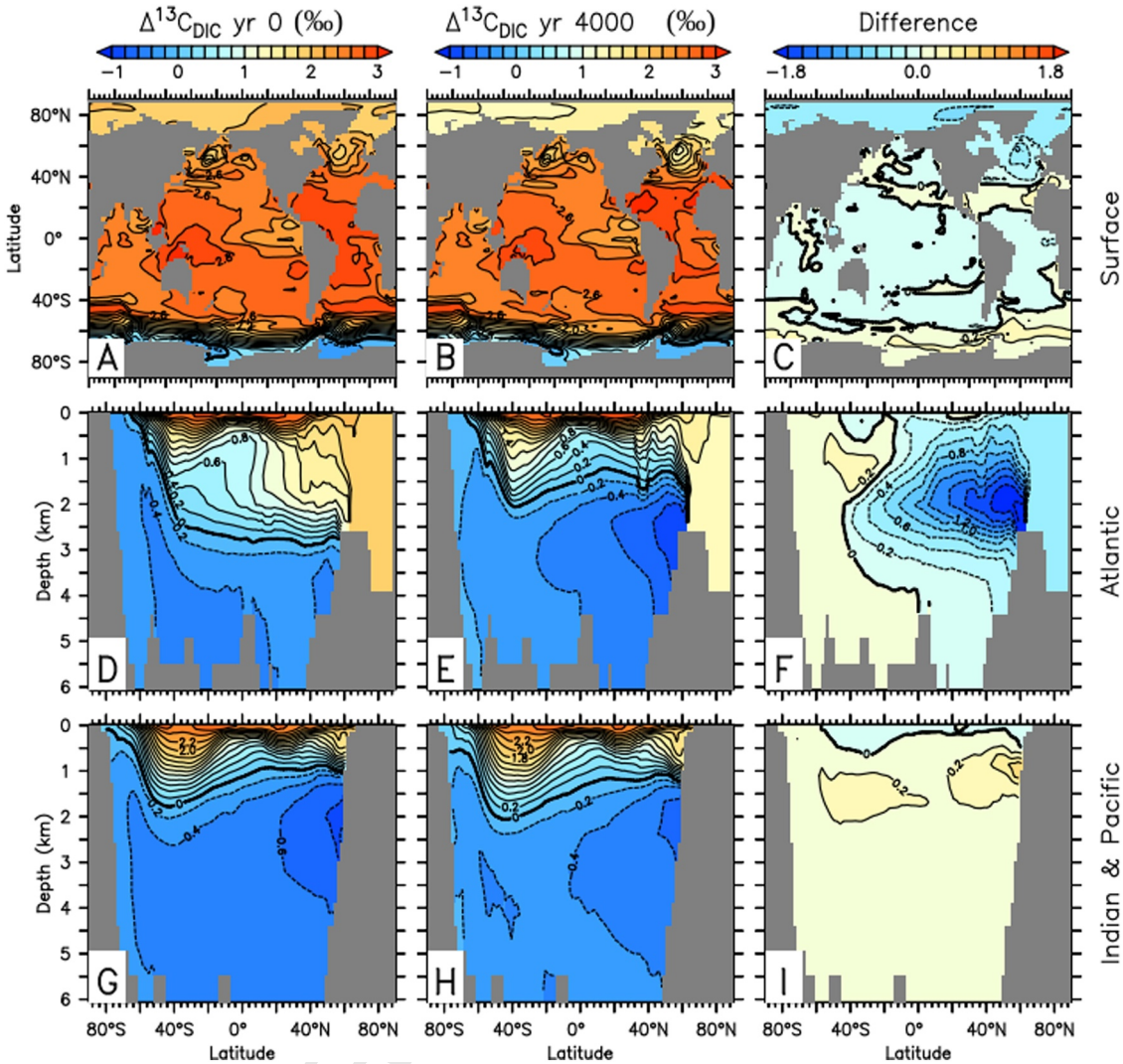

Figure 6. $\Delta^{13}C_{DIC}$ distributions at the surface (a–c) and zonally averaged sections in the Atlantic (d–f) and Indian/Pacific (g–i) in model *LGM Full* at year 0 (a, d, g), at year 4,000 (b, e, h), and the difference (year 4,000 minus year 0, c, f, i).

there. Values between 1.5 and 2.5 km depth decrease by up to 1‰, resembling the pattern of $\delta^{13}C_{DIC}$ changes (Figure 6f) but amounting to only half its amplitude. In the North Pacific $\Delta^{13}C_{soft}$ increases by up to 0.4‰, which substantially contributes to the changes of $\delta^{13}C_{DIC}$ there (Figure 6i).

3.2.4. Preformed Components

Preformed values are highest in the low-latitude surface ocean and smallest in deep waters of southern origin (Figure 9). Since deep water in the North Atlantic is advected from surface waters with much higher $\Delta^{13}C_{pre}$ at year 0, $\Delta^{13}C_{pre}$ is larger in the upper North Atlantic than in the North Pacific. The AMOC collapse decreases these differences. $\Delta^{13}C_{pre}$ values in the North Atlantic around 2 km depth decrease by up to 1‰, while they increase in much of the Indian and Pacific oceans, although this increase is smaller in magnitude (0.1–0.2‰). $\Delta^{13}C_{pre}$ is by far the dominant component for the increase in $\delta^{13}C_{DIC}$ in deep and intermediate waters outside the Atlantic, except in the far North Pacific, where $\Delta^{13}C_{soft}$ dominates.

Saturation values are strongly temperature dependent, increasing from 1‰ in the eastern tropical Pacific to 4‰ at high latitudes (Figure 10). Those patterns are dominated by $\Delta^{13}C_{sat,phy}$ (Figure S1 in Supporting Information S1).

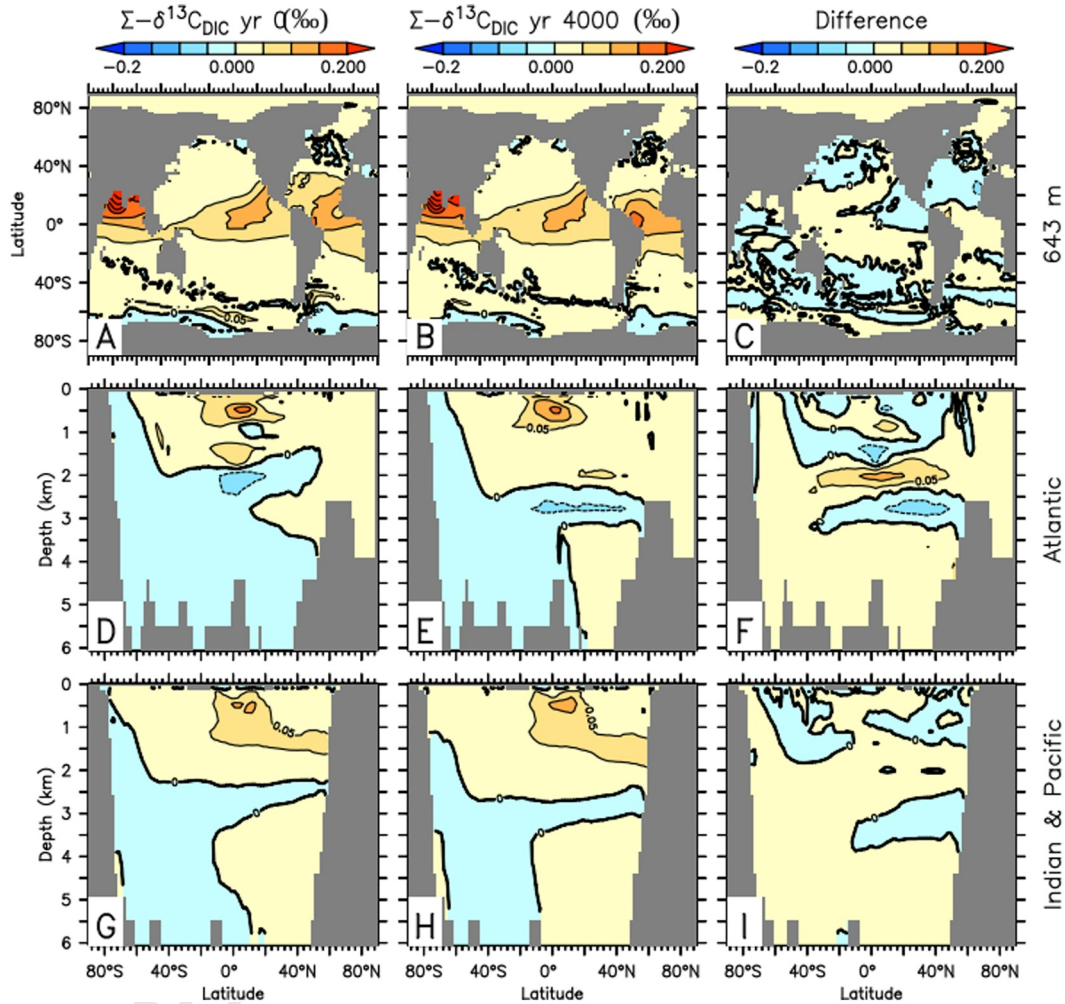

Figure 7. As Figure 6 but for error of decomposition ($^{13}\Sigma - \delta^{13}C_{DIC}$). (a–c) Maps at 643 m depth close to the maximum error in (d). Note the different range of color scale compared with Figure 6.

Changes in saturation values due to the collapse of the AMOC in model *LGM Full* are small everywhere except in the North Atlantic at 2 km depth where they decrease by −0.3‰, which is due to the biological saturation component (Figure S2 in Supporting Information S1).

In contrast, changes in disequilibrium are greater, contributing up to 0.6‰ to the decrease in $\Delta^{13}C_{pre}$ in the North Atlantic and between 0.1 and 0.2‰ to the increase in the Southern, Pacific and Indian Oceans (Figure 11). Since the disequilibrium in the North Atlantic in the case of an active AMOC at year 0 is of smaller magnitude than that of Southern Ocean waters, and both are negative, an AMOC decrease leads to a decrease in $\Delta^{13}C_{dis}$ in the North Atlantic. On the other hand, Southern Ocean waters become more equilibrated as the AMOC declines, presumably due to decreased sea ice cover, similar to the response of the disequilibrium for carbon as discussed in the companion paper (their Figure S2 in Supporting Information S1).

Whereas the biological disequilibrium is solely responsible for the decrease in $\Delta^{13}C_{dis}$ in the North Atlantic (Figure 12), both physical (Figure 13) and biological disequilibria contribute to the increase in the Indian, Southern, and Pacific Oceans. Even though changes in physical disequilibrium are relatively small everywhere, they dominate the global changes in preformed values seen in Figure 2 since they are positive almost everywhere, whereas the biological disequilibrium shows changes of opposite sign in the Pacific and Atlantic, which cancel largely in the global mean.

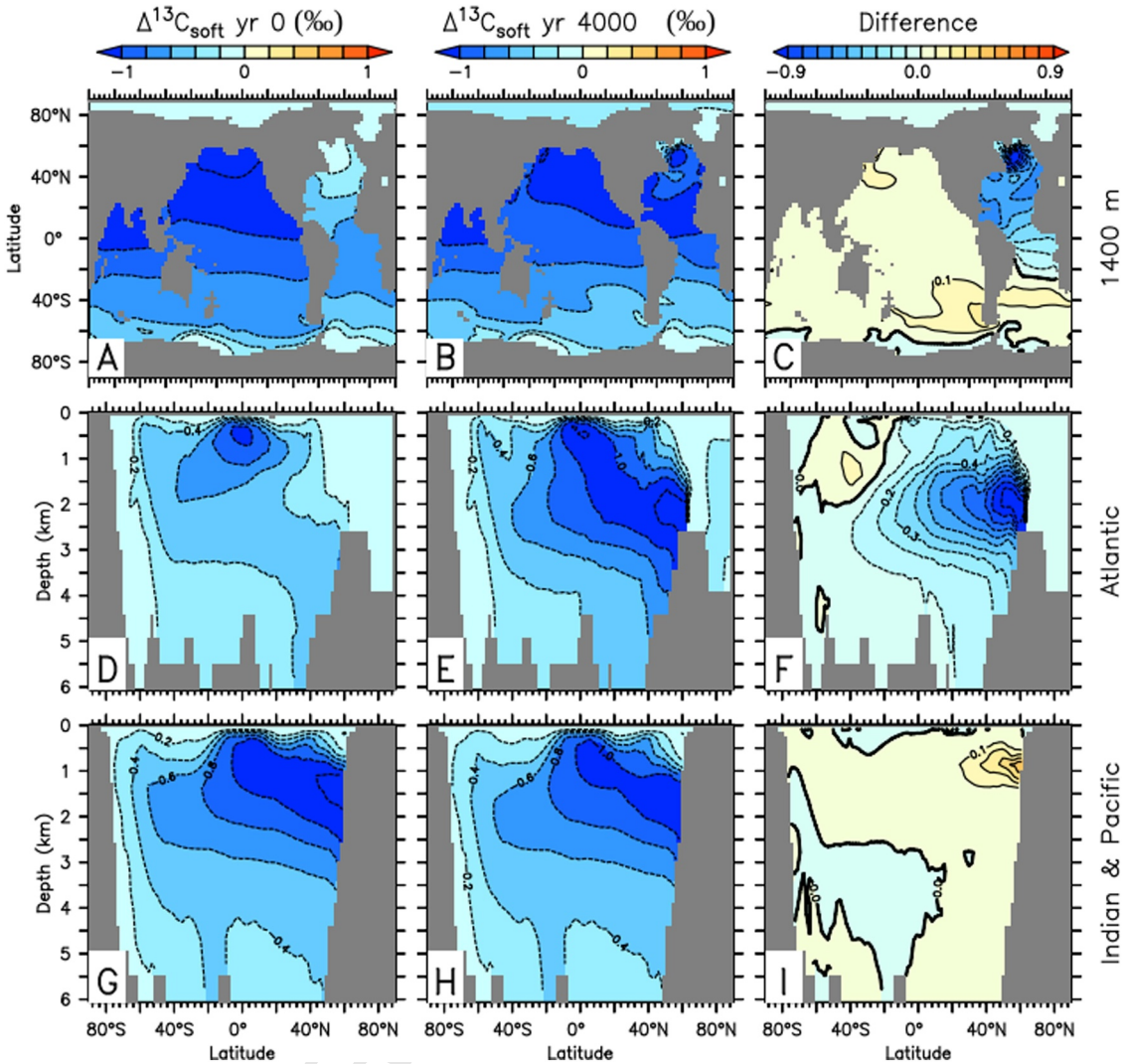

Figure 8. As Figure 6 but for the remineralized soft-tissue component $(\Delta^{13}C_{soft})$. Top row shows maps at 1,400 m. Note different range of color scale compared with Figure 6.

3.3. Simulations of AMOC Collapse Under Preindustrial Climate

Under preindustrial climate the AMOC is stronger than under LGM climate (Figure S3a in Supporting Information S1). Thus, as for carbon, changes in carbon isotopes are generally larger in the preindustrial AMOC collapse simulation (model *PI Full*) than in model *LGM Full*. $\delta^{13}C_{CO2}$ increases initially, has a rapid fluctuation around the time of the cessation of the freshwater forcing, and then decreases by about 0.2‰ by year 4,000 (Figure S3d in Supporting Information S1). In contrast to the LGM simulation (Figure 1d), $\delta^{13}C_{ocn}$ stays steady during the first 1,000 years and begins increasing afterward (Figure S3e in Supporting Information S1), while $\delta^{13}C_{lnd}$ decreases (Figure S3f in Supporting Information S1). The increase in $\delta^{13}C_{ocn}$ is driven by an increase in $\Delta^{13}C_{soft}$ (Figure S4 in Supporting Information S1) in the Pacific (Figure S6c in Supporting Information S1), whereas preformed changes in the Pacific (Figure S6b in Supporting Information S1) and globally (Figure S4b in Supporting Information S1) play a relatively smaller role than in the LGM (Figures 2 and 4).

In the Atlantic, the decrease in $\delta^{13}C_{DIC}$ extends over a broader depth range, such that zonally averaged anomalies exceed −1‰ already at a depth of about 500 m, whereas that value is reached in *LGM Full* only at 1,500 m (Figure 14 vs. Figure 5). Anomalies of −0.4‰ extend from the surface to below 3.5 km depth in *PI Full*, while in *LGM Full* that value is exceeded only from about 700 m depth to 3 km. The larger decrease in the upper ocean

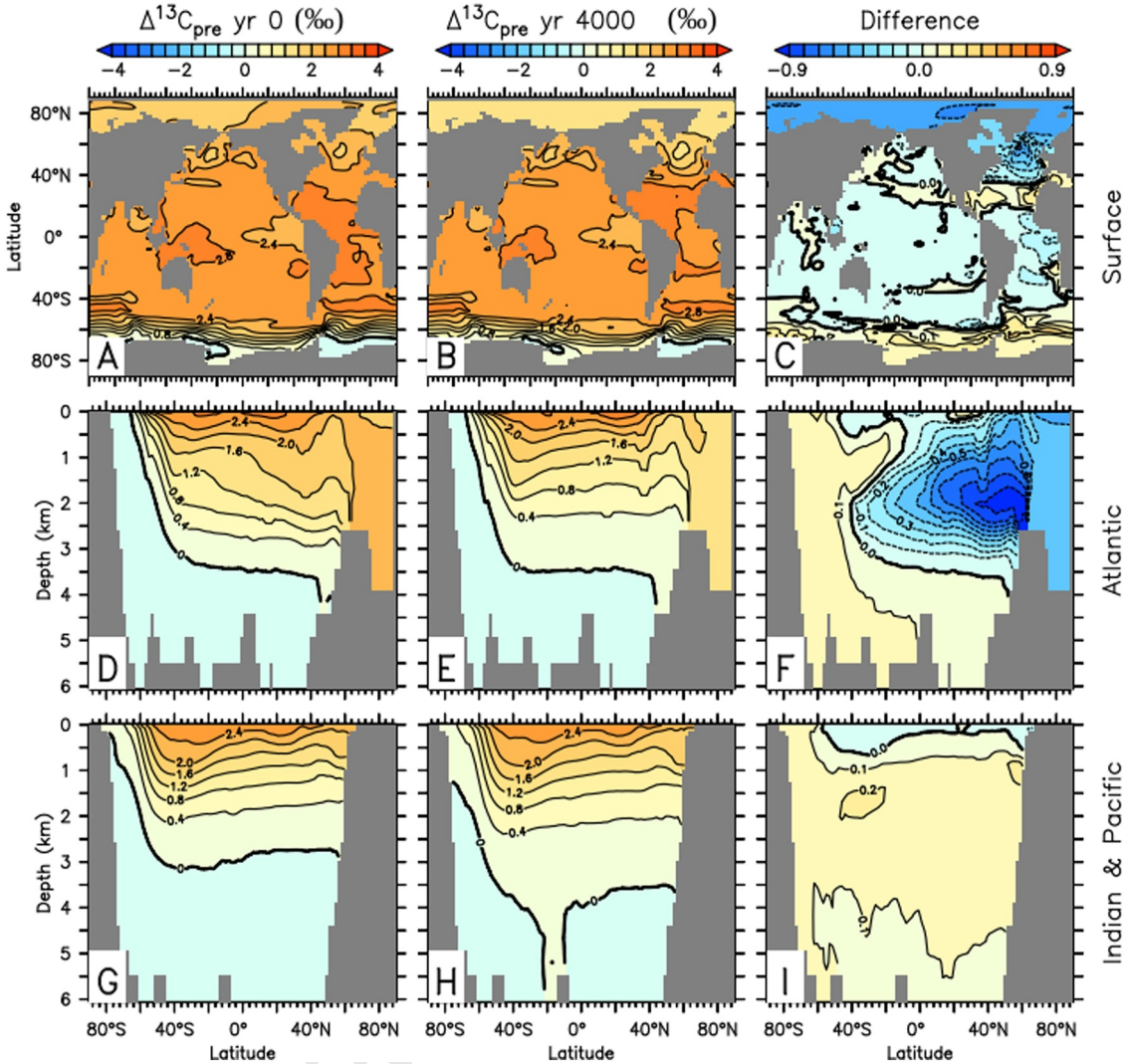

Figure 9. As Figure 8 but for the preformed component ($\Delta^{13}C_{pre}$). Top row shows surface maps.

between 500 m and 1.5 km in *PI Full* is largely due to decreases in $\Delta^{13}C_{soft}$, which contributes more than −0.7‰, while decreases in $\Delta^{13}C_{pre}$ contribute less than −0.4‰, with substantial impacts from $\Delta^{13}C_{sat}$, although the disequilibrium is the dominant contribution to $\Delta^{13}C_{pre}$ over most of the water column. In this case, the AOU approximation works remarkably well over most of the water column, except in the very deep layers below about 4 km.

In the Pacific, however, the AOU approximation overestimates the changes in $\Delta^{13}C_{soft}$, which dominates the increase in $\delta^{13}C_{DIC}$, in contrast to model *LGM Full*. Increases in $\Delta^{13}C_{soft}$ in the Pacific are larger in *PI Full* because upwelling decreases more due to the larger AMOC changes and thus productivity decreases more and remineralization of organic matter in the subsurface also decreases more compared with *LGM Full*. Preformed changes are much less important in the Pacific in *PI Full* compared with *LGM Full* (Figure 14d vs. Figure 5d) due to compensation of saturation (Figure S11i in Supporting Information S1) and disequilibrium (Figure S12i in Supporting Information S1) changes in the upper ocean.

Negative anomalies in $\delta^{13}C_{DIC}$ extend from the North Atlantic into the Arctic in *PI Full* (Figure S7f in Supporting Information S1) in contrast to *LGM Full* (Figure 6f), due to sea ice free conditions, which allow photosynthesis and accumulation of organic matter there (Figure S8 in Supporting Information S1 vs. Figure 8).

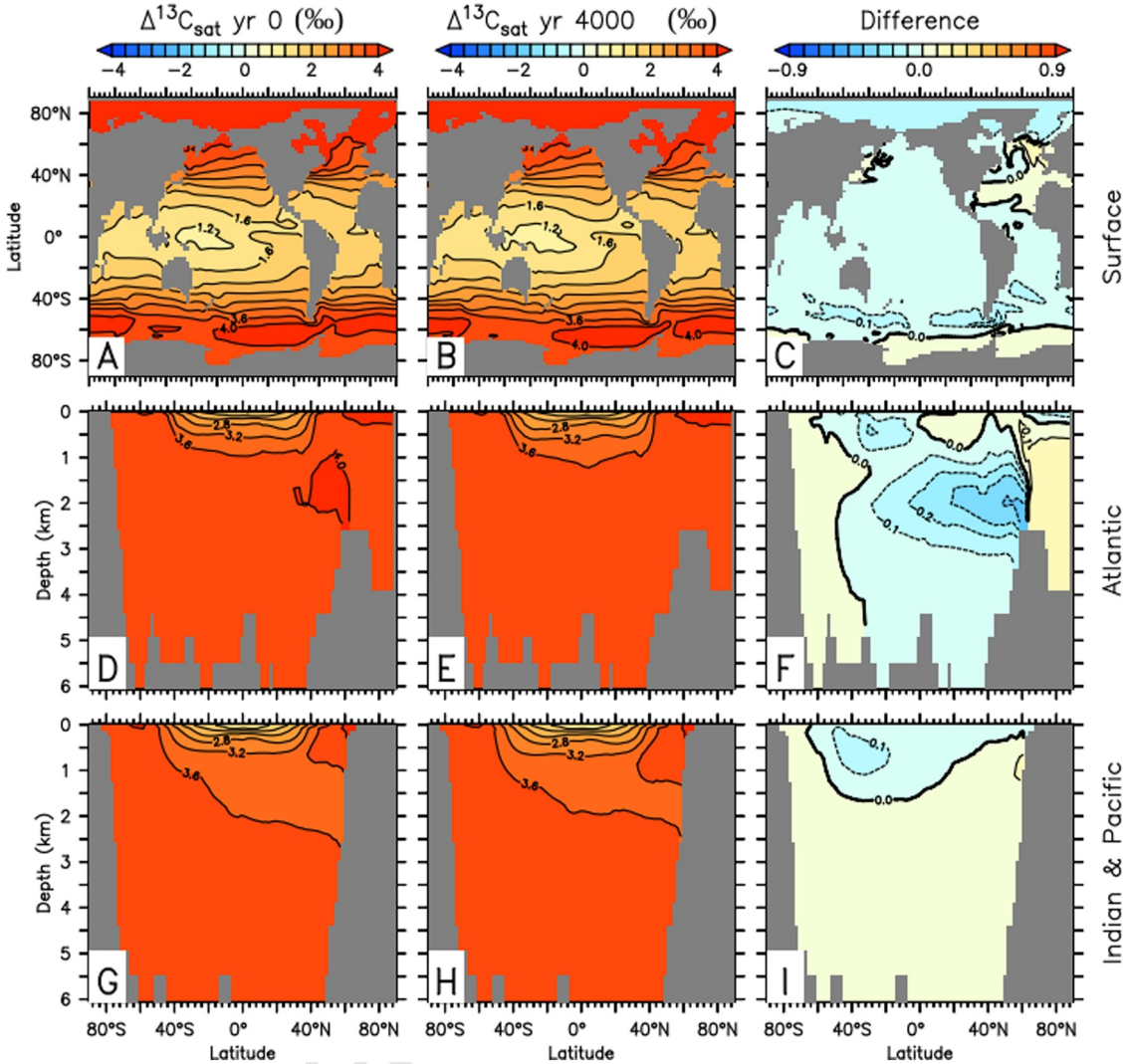

Figure 10. As Figure 8 but for the saturation component ($\Delta^{13}C_{sat}$).

4. Discussion

The AOU approximation leads to large errors in approximating $\Delta^{13}C_{soft}$ as illustrated in Figures 2c, 3c, 4c, 5b, 5d, 14b, and 14d; Figures S4c, S5c, and S6c in Supporting Information S1, in some cases it leads to the wrong sign of the changes (Figure 2c; Figure S5c in Supporting Information S1). The reason for this is that the AOU approximation includes effects of oxygen disequilibrium. Oxygen is substantially undersaturated in high-latitude surface waters (e.g., Figure S4 in Khatiwala et al., 2019), which leads to overestimation of respired carbon by the AOU approximation (Ito et al., 2004) and thus $\Delta^{13}C_{soft,AOU} < \Delta^{13}C_{soft}$ (Figure 2b in Schmittner & Fillman, 2024). This suggests that previous results based on the AOU approximation (e.g., Vollmer et al., 2022) need to be reassessed.

Similar, albeit larger, drops in $\delta^{13}C_{CO2}$ as the ones simulated in models *LGM Full* and *LGM NoBio* around year 500 (Figure 1d) have been observed on centennial timescales during the last deglaciation (Bauska et al., 2016). Overall, $\delta^{13}C_{CO2}$ changes are with ∼0.06‰ smaller than those observed on millennial scales during Marine Isotope Stage (MIS) 3 (48–35 ka; ∼0.2‰) (Bauska et al., 2018). However, the simulated CO_2 changes are also smaller than the ∼20 ppm observed, whereas the $\delta^{13}C_{CO2}/CO_2$ relationship in model *Full* is similar to that of the observations (Figure 15).

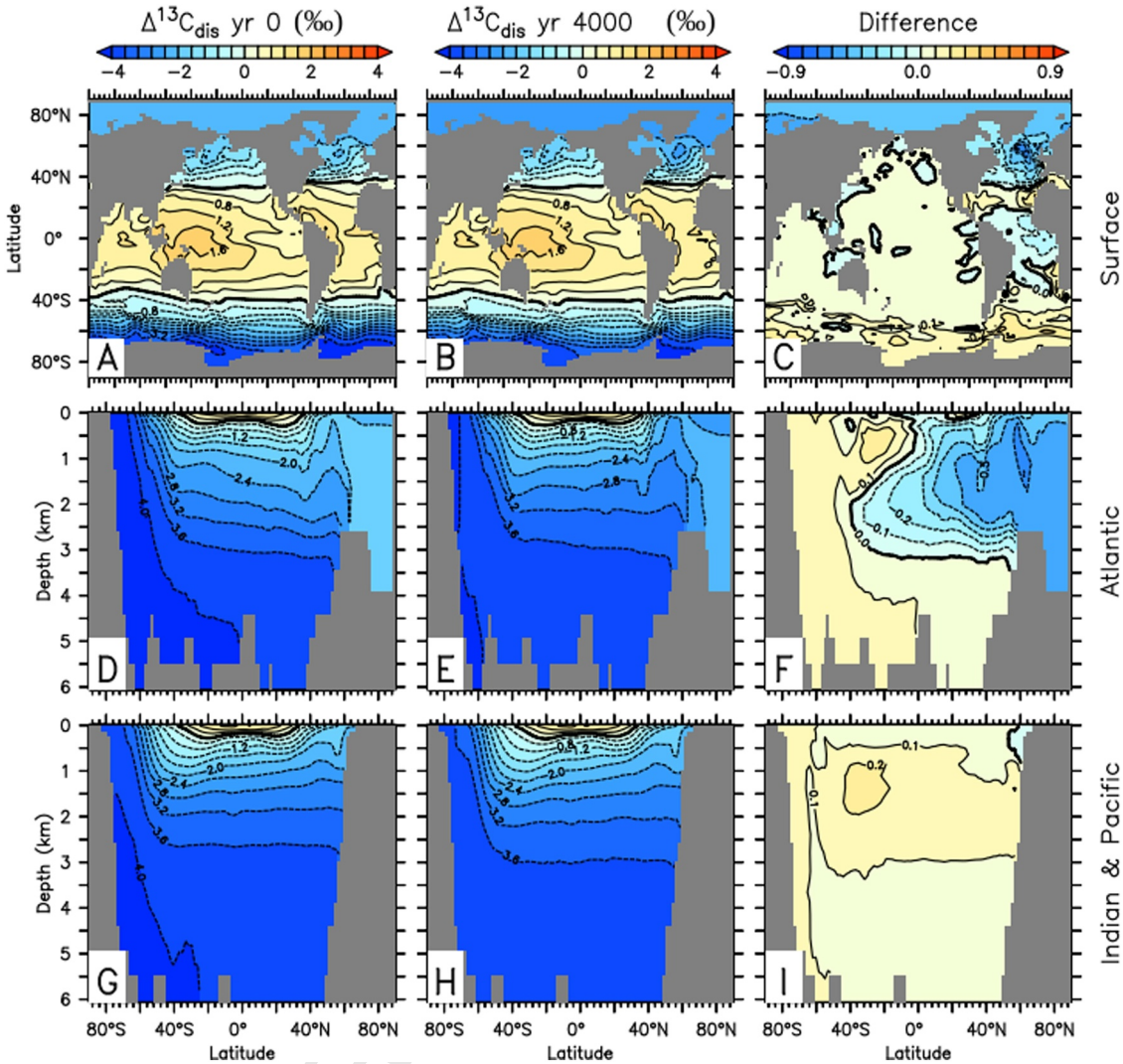

Figure 11. As Figure 8 but for the disequilibrium component ($\Delta^{13}C_{dis}$).

The relationship $\delta^{13}C_{CO2}$ versus CO_2 in the model *LGM Full* shown in Figure 15 revolves mainly along a slope of about (−0.1‰)/(10 ppm) as in the MIS3 observations (Bauska et al., 2018). However, the rapid drop around the year 500 is associated with a much steeper slope, which is absent in model *LGM NoLand*, but which has been detected in observations from the last deglaciation (Bauska et al., 2016) and which is present in model *LGM NoBio*. These results support the interpretation of Bauska et al. (2018) that millennial-scale changes during MIS3 were caused by changes in biological carbon storage in the ocean, while some of the rapid drops in $\delta^{13}C_{CO2}$ associated with steep $\delta^{13}C_{CO2}/CO_2$ slopes were caused by terrestrial carbon fluctuations.

Further exploration of changes around cessation of the freshwater fluxes (Figure 16) illustrates that after year 500, CO_2 increases by 0.56 ppm in 20 years, $\delta^{13}C_{CO2}$ decreases by 0.038‰, soil temperature, soil respiration, and NPP all increase rapidly, while the net carbon balance of the land biosphere (NPP-SR) decreases. This indicates that warming of soil temperatures leads to an increase in soil respiration that is larger than the increase in NPP, which leads to a net loss of land carbon.

Sediment data of benthic carbon isotopes show decreases in the North Atlantic during Heinrich Stadials, which have typically been interpreted as an AMOC reduction or collapse (e.g., Fang et al., 2024; Lynch-Stieglitz et al., 2019; Muglia et al., 2023; Sarnthein et al., 2001; Shackleton et al., 2000). However, the observed

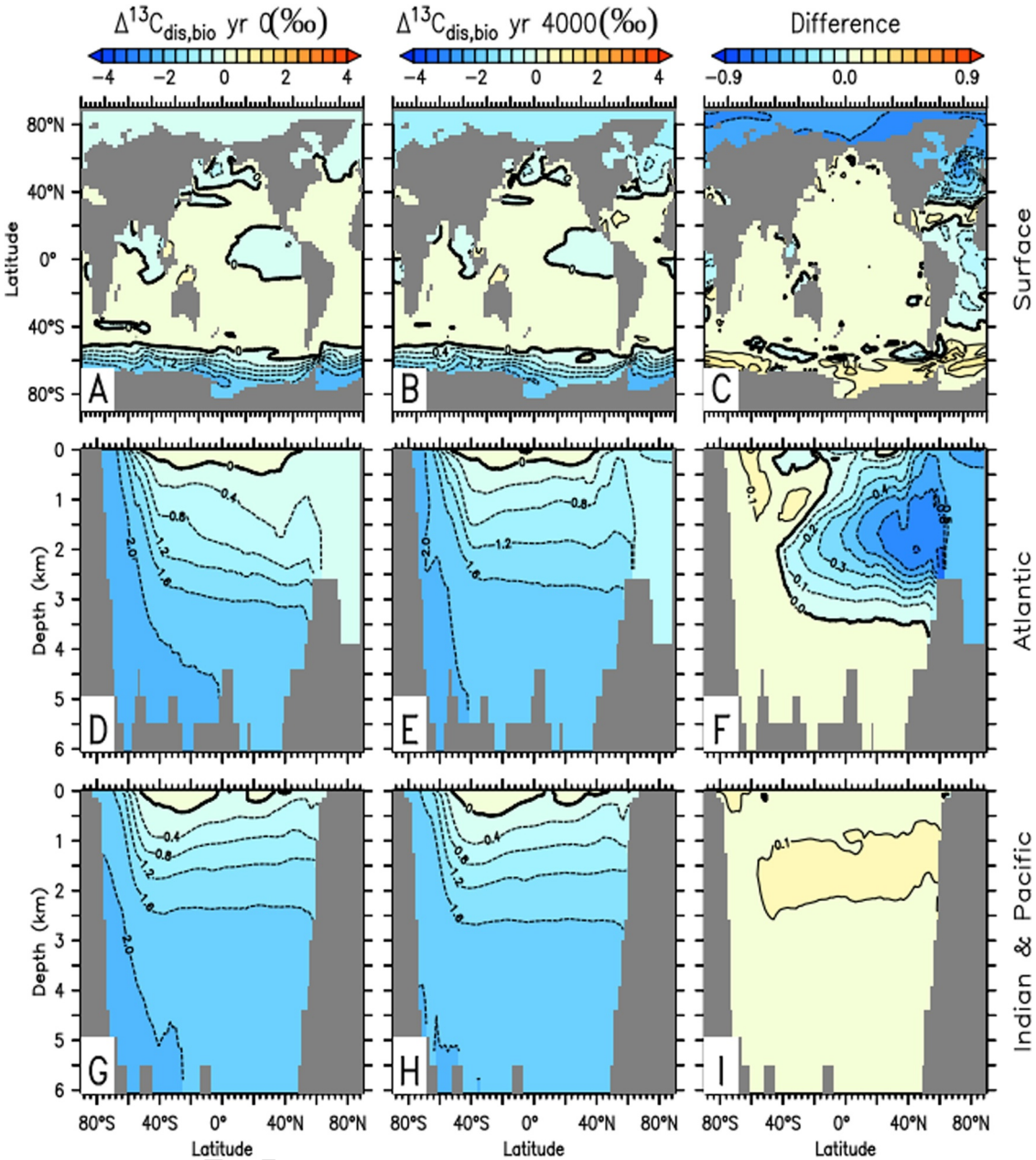

Figure 12. As Figure 8 but for biological disequilibrium carbon $(\Delta^{13}C_{dis,bio})$.

decreases are less than the 2‰ simulated in models that experience an AMOC shutdown (Figure 6; Schmittner & Lund, 2015). In models with a collapsed AMOC the carbon isotope distributions in the North Atlantic approach those in the modern North Pacific, which are much lower than what the sediment data indicate for HS1 (Pöppelmeier et al., 2023; Repschläger et al., 2021), which is why a prolonged AMOC collapse is inconsistent with those data. However, a short collapse or a reduction in strength and/or a shoaling of the AMOC could still be consistent with the sediment data. A more in-depth investigation is required to quantify the duration and severity of an AMOC reduction during HS1.

One caveat of my model simulations is that they don't include interactive sediments. Whereas I would not expect large effects of sediment interactions on the timescales discussed here, an LGM ocean with interactive sediments

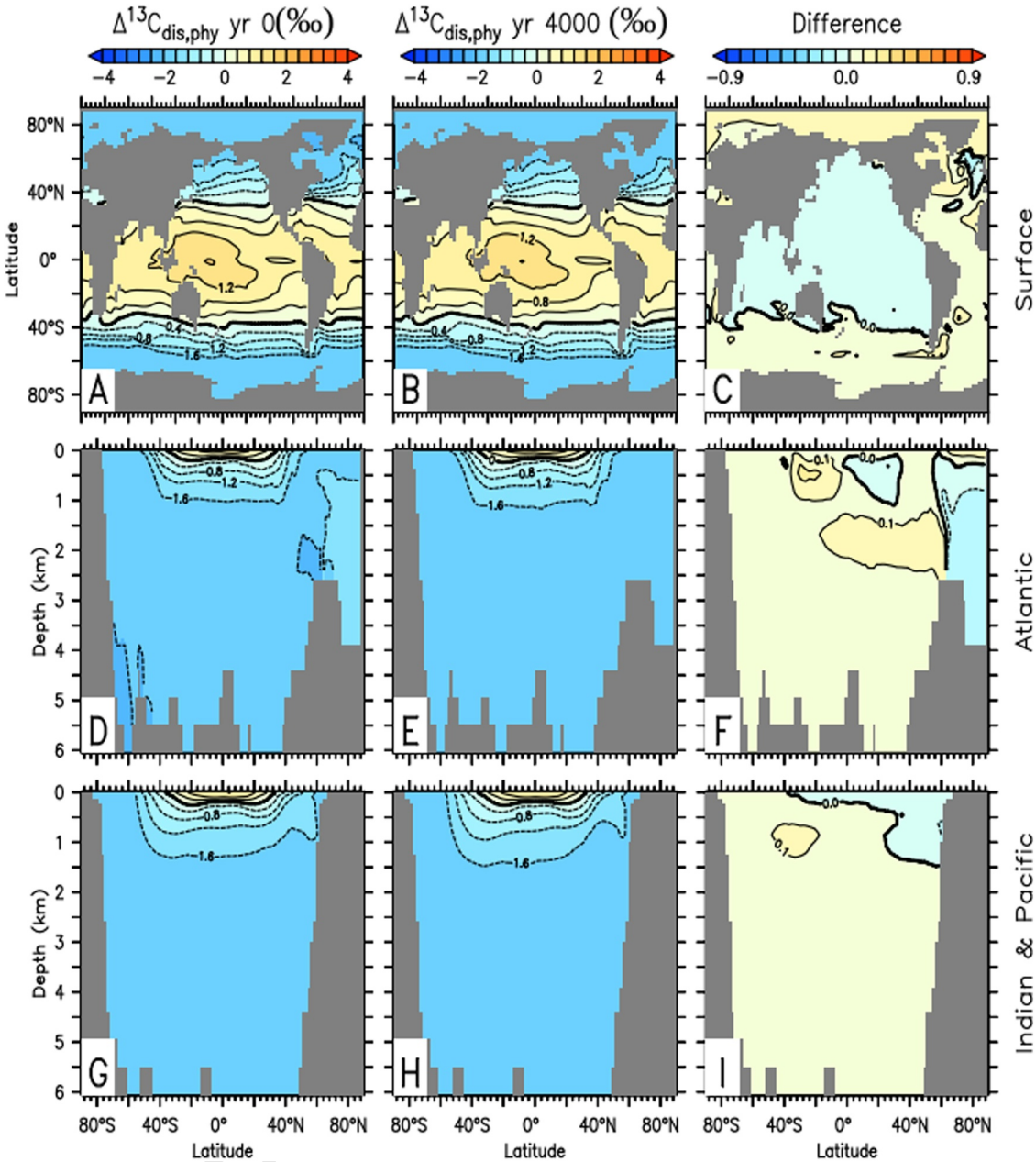

Figure 13. As Figure 8 but for physical disequilibrium carbon $\left(\Delta^{13}C_{dis,phy}\right)$.

may have a different DIC and alkalinity content. Calcium carbonate dissolution in sediments likely increased alkalinity and DIC and led to additional CO_2 drawdown from the atmosphere (Brovkin et al., 2007). Although dissolution of calcium carbonate does not affect the $\delta^{13}C_{DIC}$ significantly, the higher DIC and alkalinity content of the LGM ocean could affect air-sea gas exchange and the response of the different carbon and ^{13}C components discussed here. Although I expect those changes to be small, it would be useful to quantify their magnitude in future work.

The spin-up procedure chosen here leads to different carbon and ^{13}C inventories in the *Full* and *NoBio* runs. A different option would be to spin-up *NoBio* with prognostic (rather than fixed) CO_2 and $\delta^{13}C_{CO2}$ starting from

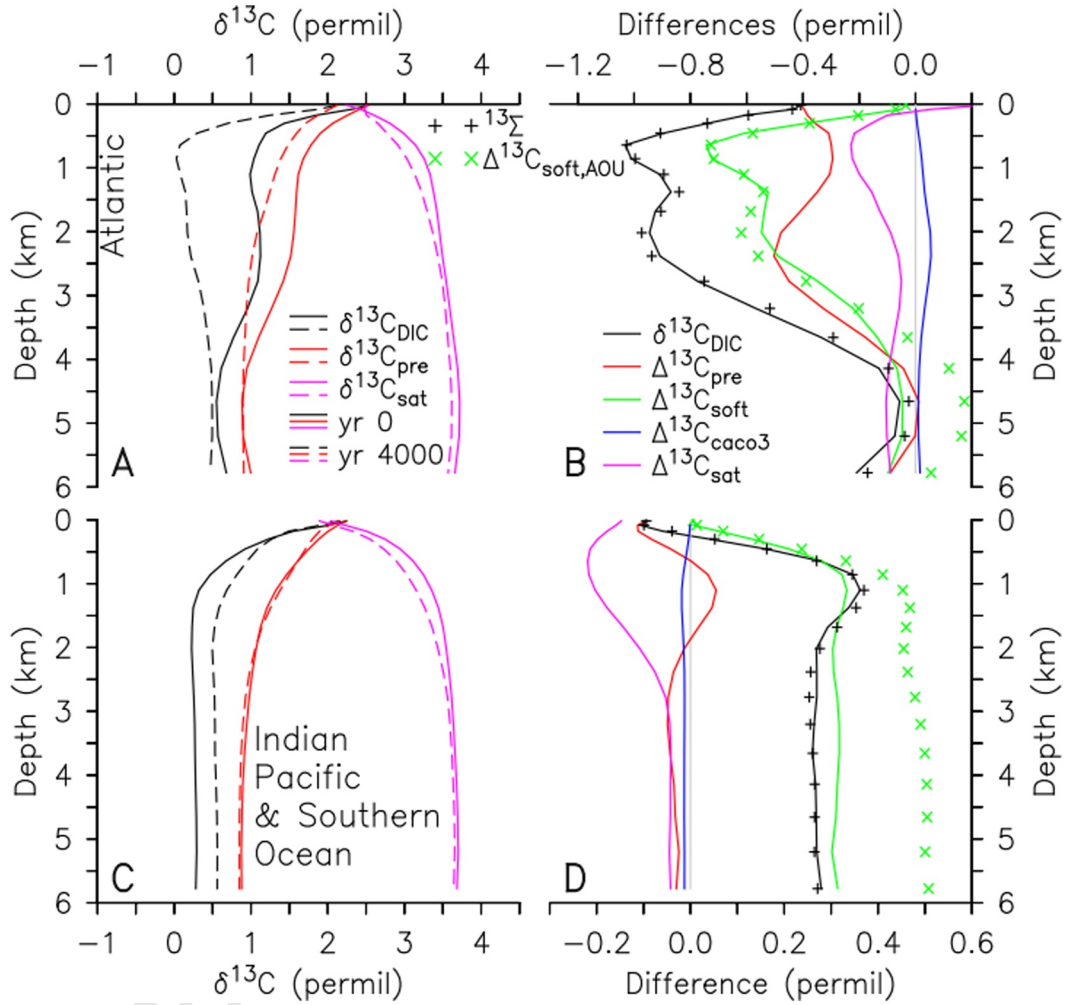

Figure 14. As Figure 5 but for model *PI Full*.

the equilibrated *Full* run, which would have led to identical inventories, but different atmospheric CO_2 and $\delta^{13}C_{CO2}$. To ensure the same climate, CO_2 in this case would have to be separated from the radiative forcing such that the climate and carbon cycle components would no longer be coupled both ways. This could presumably lead to somewhat different estimates of the biological components. Another option would be to add prognostic variables for the biological components into the model and run them simultaneously in one simulation. In this case atmospheric CO_2 and $\delta^{13}C_{CO2}$ could be identical for the *Full* and *NoBio* tracers. I expect the results for the latter option to be very similar to the ones presented here since the differences in atmospheric CO_2 and $\delta^{13}C_{CO2}$ between *Full* and *NoBio* were small and did not significantly affect climate. In summary, while I believe that our method to separate physical and biological components is logical, valid, and robust with respect to the methodology, other spin-up procedures may also be valid and should be tested and compared in the future to quantify the effects.

5. Conclusions

A simulated collapse of the AMOC leads to large decreases in $\delta^{13}C_{DIC}$ in the North Atlantic and increases in the Pacific, Indian, and Southern Oceans. Decreases in the Atlantic are similarly affected by increased accumulation of isotopically light remineralized organic matter and preformed values, both in simulations with glacial and

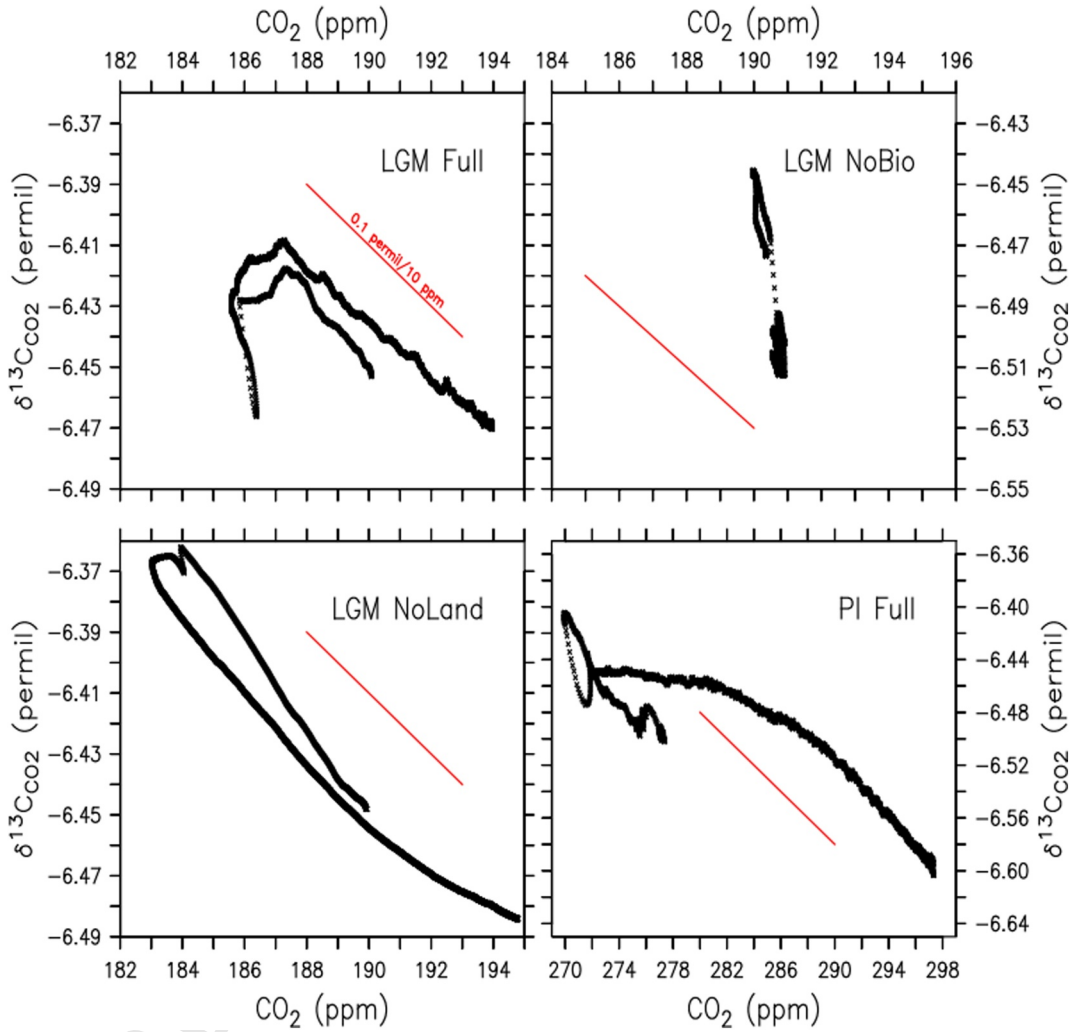

Figure 15. Scatterplots of atmospheric CO_2 versus $\delta^{13}C_{CO2}$ for models *LGM Full* (top left), *LGM NoBio* (top right), *LGM NoLand* (bottom left), and *PI Full* (bottom right). The red line indicates a slope of 0.1 permil per 10 ppm as observed during MIS3 (Bauska et al., 2018).

preindustrial conditions, contrary to the conclusions of Lacerra et al. (2017) who used the AOU approximation, which overestimates changes in $\Delta^{13}C_{soft}$ and thus underestimates changes in $\Delta^{13}C_{pre}$ (Figure 5). In our simulations, the AMOC shutdown causes a cooling of sea surface temperatures. Thus, the simulated decrease in $\delta^{13}C_{DIC}$ in the North Atlantic cannot be caused by the effect of warmer sea surface temperatures on $\Delta^{13}C_{sat}$ as suggested by Lynch-Stieglitz et al. (2019) for HS1. To the contrary, the decrease of $\Delta^{13}C_{sat}$ in our simulation is caused by the biological saturation component (Figure 10; Figure S2 in Supporting Information S1). Increases outside the Atlantic are dominated by preformed components in the glacial and remineralized components in the preindustrial simulation.

The decomposition of the ocean carbon-13 components is complete and accurate in transient simulations, supporting previous results from equilibrium simulations (Schmittner & Fillman, 2024). Thus, the method could be useful in the future in more realistic data-constrained simulations to estimate past changes in carbon isotope components.

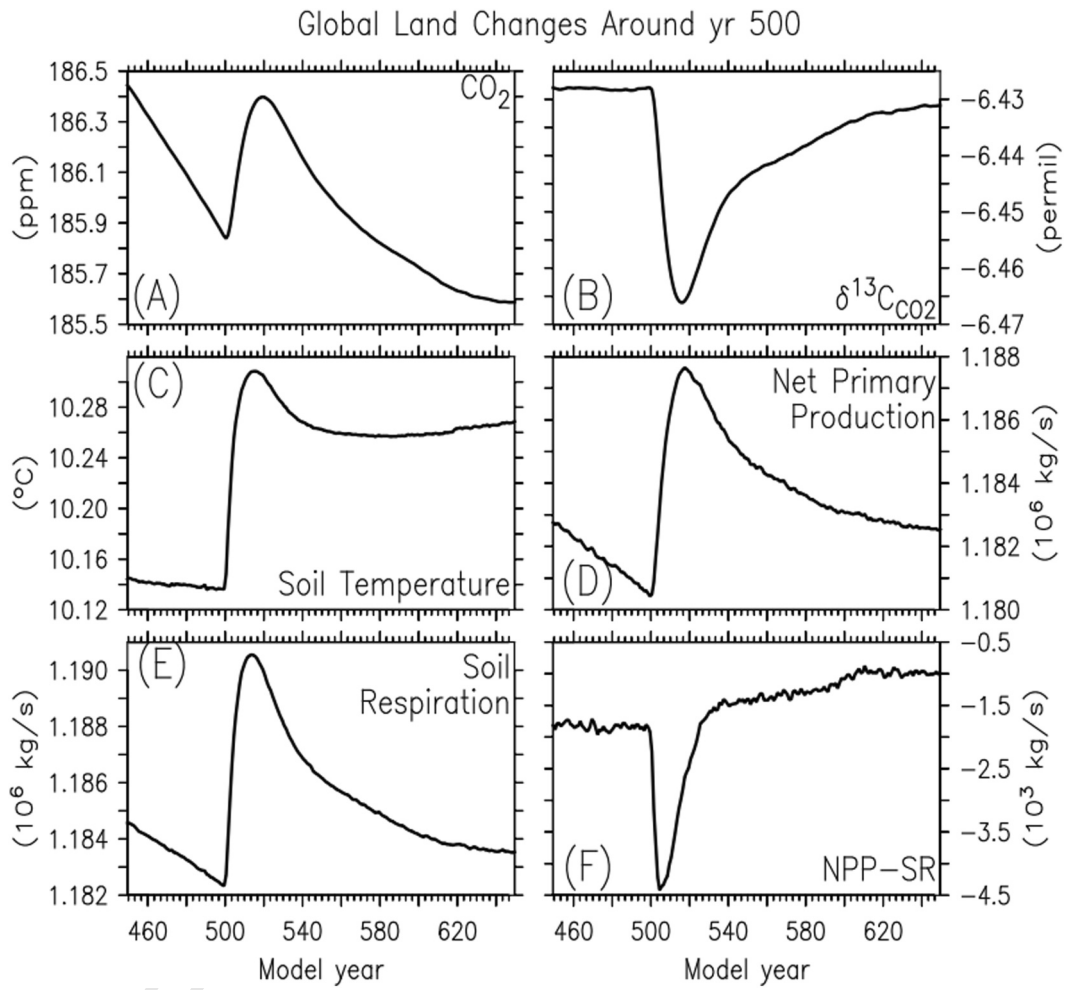

Figure 16. Timeseries of Global Changes Around Year 500 in Model *LGM Full*. (a) Atmospheric CO_2. (b) $\delta^{13}C_{CO2}$. Globally averaged soil temperature (c), Net Primary Production (NPP, d), Soil Respiration (SR, (e), and NPP-SR (f).

Conflict of Interest

The authors declare no conflicts of interest relevant to this study.

Data Availability Statement

The OSU-UVic climate model (version 2.9.10) source code is available on GitHub at https://github.com/OSU-CEOAS-Schmittner/UVic2.9/releases/tag/v2.9.10 (Schmittner, 2024b). Model code, input and output data, as well as ferret scripts to generate figures from this paper are available at Zenodo for the *LGM Full* model https://doi.org/10.5281/zenodo.14231977 (Schmittner, 2024a) and for the *PI Full* model https://zenodo.org/records/14774855 (Schmittner, 2025).

Acknowledgments
This research was supported by the US National Science Foundation Grant 1924215.

References

Ahn, J., & Brook, E. J. (2008). Atmospheric CO_2 and climate on millennial time scales during the last glacial period. *Science*, *322*(5898), 83–85. https://doi.org/10.1126/science.1160832

Ahn, J., Brook, E. J., Schmittner, A., & Kreutz, K. (2012). Abrupt change in atmospheric CO_2 during the last ice age. *Geophysical Research Letters*, *39*(18), L18711. https://doi.org/10.1029/2012GL053018

Annan, J. D., Hargreaves, J. C., & Mauritsen, T. (2022). A new global surface temperature reconstruction for the Last Glacial Maximum. *Climate of the Past*, *18*(8), 1883–1896. https://doi.org/10.5194/cp-18-1883-2022

Archer, D., Kheshgi, H., & Maier-Reimer, E. (1998). Dynamics of fossil fuel CO_2 neutralization by marine $CaCO_3$. *Global Biogeochemical Cycles*, *12*(2), 259–276. https://doi.org/10.1029/98GB00744

Bakker, P., Schmittner, A., Lenaerts, J. T. M., Abe-Ouchi, A., Bi, D., van den Broeke, M. R., et al. (2016). Fate of the Atlantic Meridional Overturning Circulation: Strong decline under continued warming and Greenland melting. *Geophysical Research Letters*, *43*(23), 12252–12260. https://doi.org/10.1002/2016GL070457

Bauska, T. K., Baggenstos, D., Brook, E. J., Mix, A. C., Marcott, S. A., Petrenko, V. V., et al. (2016). Carbon isotopes characterize rapid changes in atmospheric carbon dioxide during the last deglaciation. *Proceedings of the National Academy of Sciences of the United States of America*, *113*(13), 3465–3470. https://doi.org/10.1073/pnas.1513868113

Bauska, T. K., Brook, E. J., Marcott, S. A., Baggenstos, D., Shackleton, S., Severinghaus, J. P., & Petrenko, V. V. (2018). Controls on millennial-scale atmospheric CO_2 variability during the last glacial period. *Geophysical Research Letters*, *45*(15), 7731–7740. https://doi.org/10.1029/2018GL077881

Brovkin, V., Ganopolski, A., Archer, D., & Rahmstorf, S. (2007). Lowering of glacial atmospheric CO_2 in response to changes in oceanic circulation and marine biogeochemistry. *Paleoceanography*, *22*(4), PA4202. https://doi.org/10.1029/2006PA001380

Buizert, C., Sigl, M., Severi, M., Markle, B. R., Wettstein, J. J., McConnell, J. R., et al. (2018). Abrupt ice-age shifts in southern westerly winds and Antarctic climate forced from the North. *Nature*, *563*(7733), 681–685. https://doi.org/10.1038/s41586-018-0727-5

Buizert, C., Sowers, T. A., Niezgoda, K., Blunier, T., Gkinis, V., Harlan, M., et al. (2024). The Greenland spatial fingerprint of Dansgaard–Oeschger events in observations and models. *Proceedings of the National Academy of Sciences of the United States of America*, *121*(44), e2402637121. https://doi.org/10.1073/pnas.2402637121

Chiang, J. C. H., & Bitz, C. M. (2005). Influence of high latitude ice cover on the marine Intertropical Convergence Zone. *Climate Dynamics*, *25*(5), 477–496. https://doi.org/10.1007/s00382-005-0040-5

Fang, L., Wang, N., & Kim, M. (2024). Mapping the evolution of marine carbon during the last deglaciation: ^{13}C perspectives on the deglacial ocean carbon cycle. *Earth-Science Reviews*, *258*, 104966. https://doi.org/10.1016/j.earscirev.2024.104966

Fillman, N., Schmittner, A., & Kvale, K. F. (2023). Variable stoichiometry effects on glacial/interglacial ocean model biogeochemical cycles and carbon storage (preprint). https://doi.org/10.22541/essoar.169049091.16856096/v1

Frierson, D. M. W., Hwang, Y.-T., Fučkar, N. S., Seager, R., Kang, S. M., Donohoe, A., et al. (2013). Contribution of ocean overturning circulation to tropical rainfall peak in the Northern Hemisphere. *Nature Geoscience*, *6*(11), 940–944. https://doi.org/10.1038/ngeo1987

Gebbie, G., Peterson, C. D., Lisiecki, L. E., & Spero, H. J. (2015). Global-mean marine ^{13}C and its uncertainty in a glacial state estimate. *Quaternary Science Reviews*, *125*, 144–159. https://doi.org/10.1016/j.quascirev.2015.08.010

Ito, T., Follows, M. J., & Boyle, E. A. (2004). Is AOU a good measure of respiration in the oceans? *Geophysical Research Letters*, *31*(17), L17305. https://doi.org/10.1029/2004GL020900

Khatiwala, S., Schmittner, A., & Muglia, J. (2019). Air-sea disequilibrium enhances ocean carbon storage during glacial periods. *Science Advances*, *5*(6), eaaw4981. https://doi.org/10.1126/sciadv.aaw4981

Lacerra, M., Lund, D., Yu, J., & Schmittner, A. (2017). Carbon storage in the mid-depth Atlantic during millennial-scale climate events. *Paleoceanography*, *32*(8), 780–795. https://doi.org/10.1002/2016PA003081

Lynch-Stieglitz, J. (2017). The Atlantic Meridional Overturning Circulation and abrupt climate change. *Annual Review of Marine Science*, *9*(1), 83–104. https://doi.org/10.1146/annurev-marine-010816-060415

Lynch-Stieglitz, J., Stocker, T. F., Broecker, W. S., & Fairbanks, R. G. (1995). The influence of air-sea exchange on the isotopic composition of oceanic carbon: Observations and modeling. *Global Biogeochemical Cycles*, *9*(4), 653–665. https://doi.org/10.1029/95GB02574

Lynch-Stieglitz, J., Valley, S. G., & Schmidt, M. W. (2019). Temperature-dependent ocean–atmosphere equilibration of carbon isotopes in surface and intermediate waters over the deglaciation. *Earth and Planetary Science Letters*, *506*, 466–475. https://doi.org/10.1016/j.epsl.2018.11.024

McManus, J. F., Francois, R., Gherardi, J.-M., Keigwin, L. D., & Brown-Leger, S. (2004). Collapse and rapid resumption of Atlantic meridional circulation linked to deglacial climate changes. *Nature*, *428*(6985), 834–837. https://doi.org/10.1038/nature02494

Menking, J. A., Shackleton, S. A., Bauska, T. K., Buffen, A. M., Brook, E. J., Barker, S., et al. (2022). Multiple carbon cycle mechanisms associated with the glaciation of Marine Isotope Stage 4. *Nature Communications*, *13*(1), 5443. https://doi.org/10.1038/s41467-022-33166-3

Menviel, L., Mouchet, A., Meissner, K. J., Joos, F., & England, M. H. (2015). Impact of oceanic circulation changes on atmospheric $^{13}CO_2$. *Global Biogeochemical Cycles*, *29*(11), 1944–1961. https://doi.org/10.1002/2015GB005207

Muglia, J., Mulitza, S., Repschläger, J., Schmittner, A., Lembke-Jene, L., Lisiecki, L. E., et al. (2023). A global synthesis of high-resolution stable isotope data from benthic Foraminifera of the last deglaciation. *Scientific Data*, *10*(1), 131. https://doi.org/10.1038/s41597-023-02024-2

Muglia, J., & Schmittner, A. (2015). Glacial Atlantic overturning increased by wind stress in climate models. *Geophysical Research Letters*, *42*(22), 9862–9868. https://doi.org/10.1002/2015GL064583

Muglia, J., Somes, C. J., Nickelsen, L., & Schmittner, A. (2017). Combined effects of atmospheric and seafloor iron fluxes to the glacial ocean. *Paleoceanography*, *32*(11), 1204–1218. https://doi.org/10.1002/2016PA003077

Oppo, D. W., Curry, W. B., & McManus, J. F. (2015). What do benthic ^{13}C and ^{18}O data tell us about Atlantic circulation during Heinrich Stadial 1? *Paleoceanography*, *30*(4), 353–368. https://doi.org/10.1002/2014PA002667

Pöppelmeier, F., Jeltsch-Thömmes, A., Lippold, J., Joos, F., & Stocker, T. F. (2023). Multi-proxy constraints on Atlantic circulation dynamics since the last ice age. *Nature Geoscience*, *16*(4), 349–356. https://doi.org/10.1038/s41561-023-01140-3

Rahmstorf, S. (2024). Is the Atlantic overturning circulation approaching a tipping point? *Oceanography*, *37*(3), 16–29. https://doi.org/10.5670/oceanog.2024.501

Repschläger, J., Zhao, N., Rand, D., Lisiecki, L., Muglia, J., Mulitza, S., et al. (2021). Active North Atlantic deepwater formation during Heinrich Stadial 1. *Quaternary Science Reviews*, *270*, 107145. https://doi.org/10.1016/j.quascirev.2021.107145

Sarnthein, M., Stattegger, K., Dreger, D., Erlenkeuser, H., Grootes, P., Haupt, B. J., et al. (2001). Fundamental modes and abrupt changes in North Atlantic Circulation and Climate over the last 60 ky—Concepts, reconstruction and numerical modeling. In P. Schäfer, W. Ritzrau, M. Schlüter, & J. Thiede (Eds.), *The Northern North Atlantic: A Changing Environment* (pp. 365–410). https://doi.org/10.1007/978-3-642-56876-3_21

Schmittner, A. (2024a). OSU-UVic climate model version 2.9.10 with diagnostic tracers for carbon and carbon-13 decomposition [Software]. *Oregon State University*. Retrieved from https://github.com/OSU-CEOAS-Schmittner/UVic2.9

Schmittner, A. (2024b). OSU-UVic hosing run with LGM initial conditions (LGM Full) [Dataset]. *Zenodo*. https://doi.org/10.5281/zenodo.14231978

Schmittner, A. (2025). OSU-UVic hosing run with preindistrial initial conditions (PI Full) [Dataset]. *Zenodo*. https://doi.org/10.5281/zenodo.14774855

Schmittner, A., & Boling, M. (2025). Impact of Atlantic Meridional Overturning circulation collapse on dissolved inorganic carbon components in the ocean. *Global Biogeochemical Cycles*. submitted manuscript. https://doi.org/10.22541/essoar.173884341.17815844/v1

Schmittner, A., Brook, E. J., & Ahn, J. (2007). Impact of the ocean's overturning circulation on atmospheric CO_2. In A. Schmittner, J. C. H. Chiang, & S. R. Hemming (Eds.), *Ocean Circulation: Mechanisms and Impacts* (Vol. 173, pp. 209–246). American Geophysical Union (AGU). https://doi.org/10.1029/173gm20

Schmittner, A., & Fillman, N. J. (2024). Carbon and carbon-13 in the preindustrial and glacial ocean. *PLOS Climate*, *3*(7), e0000434. https://doi.org/10.1371/journal.pclm.0000434

Schmittner, A., Gruber, N., Mix, A. C., Key, R. M., Tagliabue, A., & Westberry, T. K. (2013). Biology and air–sea gas exchange controls on the distribution of carbon isotope ratios (^{13}C) in the ocean. *Biogeosciences*, *10*(9), 5793–5816. https://doi.org/10.5194/bg-10-5793-2013

Schmittner, A., & Lund, D. C. (2015). Early deglacial Atlantic overturning decline and its role in atmospheric CO_2 rise inferred from carbon isotopes (^{13}C). *Climate of the Past*, *11*(2), 135–152. https://doi.org/10.5194/cp-11-135-2015

Shackleton, N. J., Hall, M. A., & Vincent, E. (2000). Phase relationships between millennial-scale events 64,000–24,000 years ago. *Paleoceanography*, *15*(6), 565–569. https://doi.org/10.1029/2000PA000513

Somes, C. J., & Oschlies, A. (2015). On the influence of "non-Redfield" dissolved organic nutrient dynamics on the spatial distribution of N2 fixation and the size of the marine fixed nitrogen inventory. *Global Biogeochemical Cycles*, *29*(7), 973–993. https://doi.org/10.1002/2014GB005050

Tierney, J. E., Zhu, J., King, J., Malevich, S. B., Hakim, G. J., & Poulsen, C. J. (2020). Glacial cooling and climate sensitivity revisited. *Nature*, *584*(7822), 569–573. https://doi.org/10.1038/s41586-020-2617-x

Toggweiler, J. R., Gnanadesikan, A., Carson, S., Murnane, R., & Sarmiento, J. L. (2003a). Representation of the carbon cycle in box models and GCMs: 1. Solubility pump. *Global Biogeochemical Cycles*, *17*(1), 1026. https://doi.org/10.1029/2001GB001401

Toggweiler, J. R., Murnane, R., Carson, S., Gnanadesikan, A., & Sarmiento, J. L. (2003b). Representation of the carbon cycle in box models and GCMs, 2, Organic pump. *Global Biogeochemical Cycles*, *17*(1), 1027. https://doi.org/10.1029/2001GB001841

van Westen, R. M., Kliphuis, M., & Dijkstra, H. A. (2024). Physics-based early warning signal shows that AMOC is on tipping course. *Science Advances*, *10*(6), eadk1189. https://doi.org/10.1126/sciadv.adk1189

Vollmer, T. D., Ito, T., & Lynch-Stieglitz, J. (2022). Proxy-based preformed phosphate estimates point to increased biological pump efficiency as primary cause of last glacial maximum CO_2 drawdown. *Paleoceanography and Paleoclimatology*, *37*(11), e2021PA004339. https://doi.org/10.1029/2021PA004339

Weaver, A. J., Eby, M., Wiebe, E. C., Bitz, C. M., Duffy, P. B., Ewen, T. L., et al. (2001). The UVic earth system climate model: Model description, climatology, and applications to past, present and future climates. *Atmosphere-Ocean*, *39*(4), 361–428. https://doi.org/10.1080/07055900.2001.9649686

Weijer, W., Cheng, W., Garuba, O. A., Hu, A., & Nadiga, B. T. (2020). CMIP6 models predict significant 21st century decline of the Atlantic Meridional Overturning Circulation. *Geophysical Research Letters*, *47*(12), e2019GL086075. https://doi.org/10.1029/2019GL086075

Zhang, J., Quay, P. D., & Wilbur, D. O. (1995). Carbon isotope fractionation during gas-water exchange and dissolution of CO_2. *Geochimica et Cosmochimica Acta*, *59*(1), 107–114. https://doi.org/10.1016/0016-7037(95)91550-D